Title: Single-blind validation of space-based point-source methane emissions detection and quantification

Authors: Evan D. Sherwin[1,*], Jeffrey S. Rutherford[1], Yuanlei Chen[1], Sam Aminfard[2], Eric A. Kort[3], Robert B. Jackson[4], Adam R. Brandt[1]

Author Affiliations:

[1] Department of Energy Resources Engineering, Stanford University, Stanford, California 94305, United States

[2] ExxonMobil Upstream Research Company, Spring, Texas 77389, United States

[3] Climate and Space Sciences and Engineering, University of Michigan, Ann Arbor, Michigan 48109, United States

[4] Earth System Science, Woods Institute for the Environment and Precourt Institute for Energy, Stanford University, Stanford, California 94305, United States

[*] Correspondence: evands@stanford.edu

Abstract

Satellites are increasingly seen as a tool for identifying large greenhouse gas point sources for mitigation, but independent verification of satellite performance is needed for acceptance and use by policy makers and stakeholders. We conduct to our knowledge the first single-blind controlled methane release testing of satellite-based methane emissions detection and quantification, with five independent teams analyzing data from one to five satellites each. Teams correctly identified 71% of all emissions, ranging from 0.20 [0.19, 0.21] metric tons per hour (t/h) to 7.2 [6.8, 7.6] t/h. Over three-quarters (78%) of quantified estimates fell within ±50% of the metered value, comparable to airplane-based remote sensing technologies. The relatively wide-area Sentinel-2 and Landsat 8 satellites detected emissions as low as 1.4 [1.3, 1.5, 95% confidence interval] t/h, while GHGSat's targeted system quantified an 0.20 [0.19, 0.21] t/h emission to within 13%. While the fraction of global methane emissions detectable by satellite remains unknown, we estimate that satellite networks could see 18-81% of total oil and natural gas system emissions detected in a recent survey of a high-emitting basin.

Keywords:
Methane, hyperspectral imaging, remote sensing, satellite, single-blind, controlled release

Cutting anthropogenic methane emissions is a major near-term greenhouse gas (GHG) reduction option, often with low or negative net cost [1,2]. Recent data from aircraft and satellite surveys suggest that these emissions are substantially larger than previously thought (*3*–*6*). The outsized role of rare, very large point-source emissions has been demonstrated in multiple studies, particularly in fast-growing, oil-rich regions such as the United States Permian Basin (*4*, *5*, *7*, *8*). Major emissions, with magnitudes of metric tons of methane per hour or higher, have been seen around the world, with large sources identified in oil and gas producing regions for which there was previously little to no published methane data *(5)*.

Satellite-based methane sensing technologies have the potential to identify large methane emissions from multiple sectors quickly across the globe and flag them for repair or mitigation. Tiered networks of satellite-based methane sensors will allow rapid identification of the largest emissions. Lower-resolution configurations can automatically survey most of Earth's land area over some regular period of time. High-resolution point-and-shoot satellites, with a smaller targeted field of view, allow more sensitive investigation of specific infrastructure that may be likely to emit methane. Satellites are thus uniquely poised to contribute toward independently assessing compliance with national and international methane reduction commitments such as the Global Methane Pledge [3].

Growing efforts have therefore arisen to develop satellite-based methane-sensing technologies, moving rapidly from detecting whole-field emissions [4] to identifying point-source emissions from individual facilities [5–9]. Large investments are therefore being made in satellite networks due to launch in coming years [10]. In addition, data from some pre-existing satellite networks such as Sentinel-2 and Landsat 8 have been repurposed to detect methane, facilitating retrospective analysis of historical methane emissions across the globe [5,11,12].

Establishing a multi-stakeholder consensus over the capabilities of methane-sensing satellites is critical for integrating them into national and international methane policy and accounting. For

example, efforts by countries to assess and reduce the greenhouse gas intensity of imported fossil fuels could rely on satellites in regions where deployment of ground-based or aerial technologies would be difficult. Other potential uses include domestic identification and assessment of greenhouse gas emissions, and validation of atmospheric models of methane sources and sinks.

Existing satellite validation efforts largely focus on the consistency of quantification estimates across satellites and methods [5,11,13], or rely on internal and generally unpublished controlled methane release testing. Although independent blind testing has become commonplace for terrestrial and airborne methane sensing technologies, to our knowledge there has until now been no such testing of the methane detection and quantification capabilities of satellites [14–16]. This is largely due to the expense and logistical challenges of performing releases at scales visible from space (100s to 1,000s of kg CH_4 per hour).

1. Single-blind testing

To provide such validation, we employed a fixed-location single-blind experimental design to test point-source methane sensing systems. Participating teams were aware of the existence, timeframe, and rough location of the test, but were not informed of the size of the emissions released or the precise configuration of equipment on the ground. Large volumes of methane were released from a metered stack, after regassification from a liquified natural gas (LNG) truck. Releases were performed in Ehrenberg, Arizona, United States over a 19-day period from October 16 to November 3, 2021 (see Materials and Methods).

Metered controlled release volumes – including zero-volume releases – were retained by our team and not given to participating analysts until all estimates were submitted by all teams for all stages of the test. Analysts estimated methane emissions for each overpass, with reporting in compliance with the Advancing Development of Emissions Detection protocol for airplane and satellite systems [17].

We performed releases during overpasses of five satellites: the commercial GHGSat C2 (GSC2) and WorldView 3 (WV3) instruments, and the publicly-funded Sentinel-2, Landsat 8 (LS8), and PRISMA satellites. With the exception of GHGSat C2, none of these satellites was explicitly designed for methane sensing, but their data have instead been repurposed to this end. Analysts first attempted to estimate emissions volumes using available data from satellites and wind reanalysis products. In some cases, multiple teams assessed the same observation from an instrument, giving us the ability to empirically assess variability derived purely from the measured spectra and source quantification algorithms, which participating teams were not required to release. See the SI, Section S3 for the details each team elected to share about their algorithms.

The fact that all tested methane-sensing satellites rely on reflected sunlight introduces design trade-offs between spatial coverage, revisit frequency, and sensor resolution, compounded by the fact that most of these satellites were not designed for methane point source sensing. These tradeoffs are illustrated in Table 1. For example, the TROPOMI instrument of the Sentinel-5P satellite achieves global coverage with daily revisit time, but primarily detects emissions of 10

metric tons of methane per hour or greater (hereafter t/h, measured on mass of methane basis unless otherwise stated). This is due to the large effective pixel size of the TROPOMI instrument, roughly 7x7 km [8]. Sentinel-2 and Landsat 8 passively cover nearly the entire world's landmass with per-satellite revisit times of 10 and 16 days, respectively, with teams reanalyzing these data advertising minimum detection limits of 1-3 t/h [5,13]. GHGSat, PRISMA, and WorldView 3 are targeted "point-and-shoot" instruments, facilitating minimum detection levels claimed to be as low as 0.1 t/h at the expense of comprehensive spatial coverage [9,18,19]. In principle, all of the satellites have the theoretical ability to observe over most of Earth's land area when sufficient solar radiance is present. See SI Section S2 for further discussion of each satellite.

Table 1. Key characteristics of each participating satellite constellation, from lowest to highest swath width, which is roughly proportional to an instrument's minimum methane detection limit. Global coverage refers to a configuration that passively covers most of Earth's surface over some number of orbits, while targeted coverage refers to a "point-and-shoot" instrument that must be pointed to a particular location.

Satellite	Spectral bands	Coverage	Constellation size	Swath [km]	~Revisit time (per satellite)	Data availability
GHGSat-C2 [18]	Multi-spectral	Targeted	5 (C1-C5)*	12	14 days	Commercial
WorldView 3 [20]	Multi-spectral	Targeted	1	13.1	4.5 days‡	Commercial
PRISMA [21]	Hyperspectral	Targeted	1	3	7 days	Public
Landsat-8 [22]	Multi-spectral	Global	1	185	16 days	Public
Sentinel-2 [23]	Multi-spectral	Global	2	290	10 days	Public

*GHGSat C3-C5 were launched after the conclusion of testing.
‡For best resolution within 20° off nadir. WorldView 3 has 1-day revisit time at lower guaranteed resolution.

Participating analysis teams include private companies GHGSat [24] and Kayrros [25], as well as government research institution Stichting Ruimte Onderzoek Nederland (SRON) [26,27] and university researchers from Universitat Politècnica de València (Luís Guanter, Itziar Irakulis Loitxate, Elena Sánchez García, and Javier Gorroño Viñegla [11,28–30]) and Harvard University (Daniel Varon [5,7,31]). Each analysis team had the opportunity to submit estimates for all satellites tested, with the exception of GHGSat C2, to which GHGSat had sole access. See the SI, Section S3 for a description of each team and its members.

Following completion of the testing, methane emission estimates were submitted by participating teams in two rounds in a staged unblinding process. In stage 1 of the assessment, participating teams were provided times of releases and analyzed the associated satellite image data without access to any ground-based meteorological measurements using only rough coordinates for the release location, accurate to within 150 m. After submitting these stage 1 estimates, teams received unblinded 10-m ultrasonic anemometer wind measurements (1 Hz) from the experimental site and the precise coordinates of the release point. The teams then used the measured wind vector and release point coordinates to make updated stage 2 estimates to assess resulting accuracy gains. See supplementary information (SI) Sections S2, S3 and S4 for further discussion of participating teams, the experimental design, and materials and methods employed during testing, respectively.

Results

Of the 49 reported estimates from five teams, 35 (71%) were correctly identified, either as a true positive detection or a true negative in which no methane was emitted or detected (Figure 1). Furthermore, there were no false positives, in which a satellite incorrectly reported the presence of methane when no release occurred. In all cases, emissions seen ranged from metered values of 1.4 [1.3, 1.5, 95% confidence interval] to 7.2 [6.9, 7.6] t/h with the exception of GHGSat, with a minimum metered release level of 0.20 [0.19, 0.21] t/h. A single release value of 0 t/h, given to Sentinel-2, was correctly identified by all three teams as a non-emission event. A total of 8 cases (16%) resulted in filtered retrievals in which no estimate was attempted due either to unfavorable weather conditions, particularly heavy cloud cover, which blocks transmission of the required infrared light, or due to image clipping concerns. This highlights that even in the US desert Southwest, cloud cover can be a limiting factor for satellites. In 4 cases (8%), satellites passed over but were not tasked due to internal scheduling issues on the satellite side, with no data collected as a result.

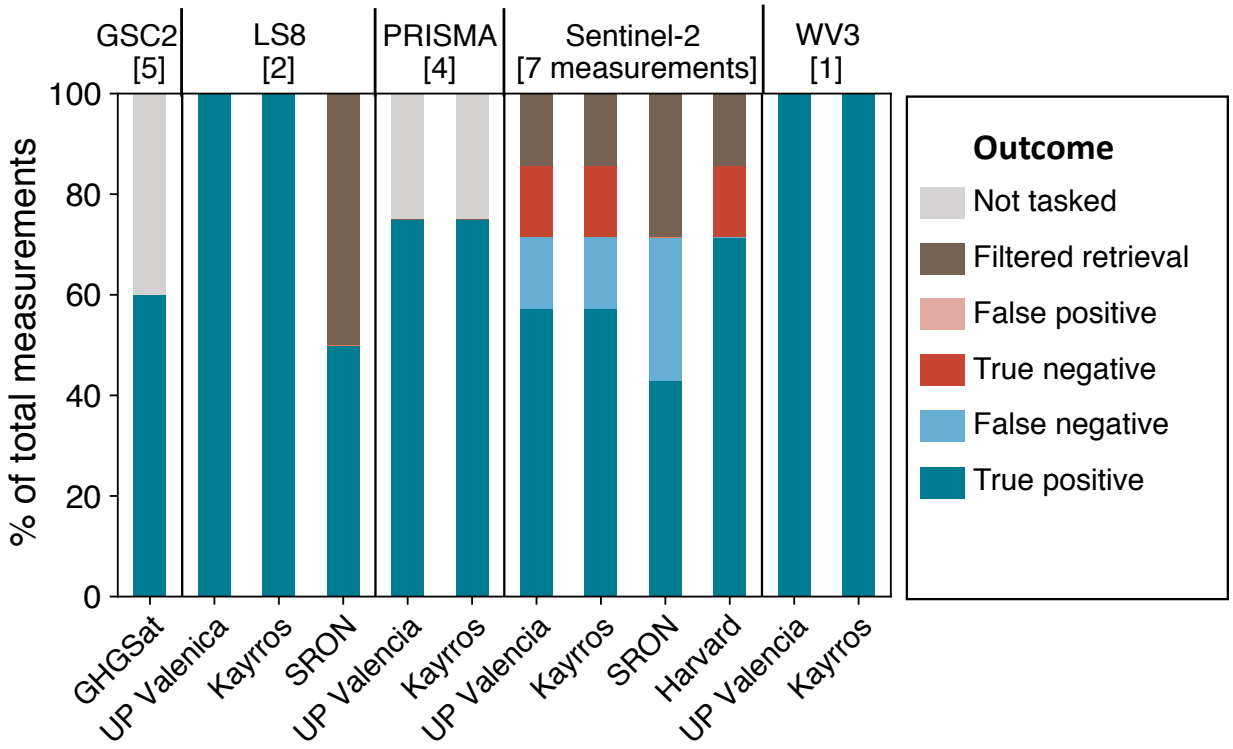

Figure 1. Detection performance by satellite and team. Total number of measurements listed in brackets. For each satellite, most teams correctly detected most emissions as true positives or true negatives (correctly identified non-emissions). In some cases, e.g. one GHGSat C2 (GSC2) overpass, the satellite was not tasked and collected no data. In others, e.g. one SRON retrieval of Landsat 8 (LS8), no retrieval was attempted due to image clipping concerns or excessive cloud cover. No teams produced false positives, in which satellites detected methane when none was released.

While methane-release volumes were randomized, each satellite was given at least one release in the 4 t/h range (3.6-4.5 t/h), measured as the average flow rate over 300 seconds prior to

overpass, accounting for uncertainty as described in Materials and Methods. All teams were able to correctly detect these emissions, with false-color methane plume images shown in Figure 2, with each team applying the same color scale for methane enhancement. Although each image shows an emission of similar magnitude, the plume appears much larger and longer for more sensitive instruments, such as GHGSat C2 and PRISMA than for less sensitive instruments, such as Sentinel-2 and Landsat 8. Estimated mean emission rate for each team and 10-m one-minute average measured wind speed and direction are inset in white.

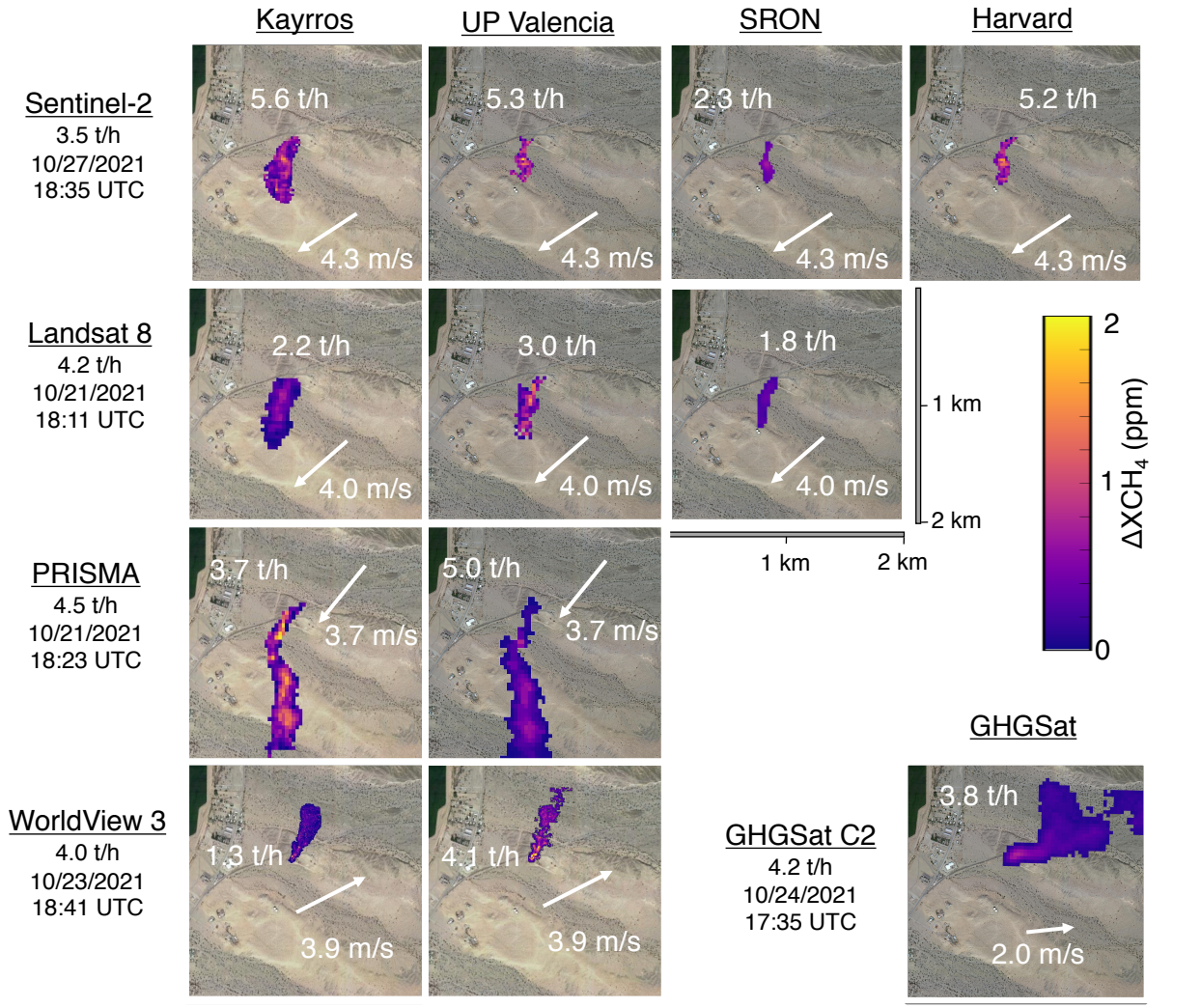

Figure 2. Visualization of detected emissions for all satellite-team combinations for mean metered release values in the 4 t/h approximate range (3.6-4.5 t/h). The true measured emissions rate and timestamp are given below satellite name. Mean estimated volume from each team/satellite pair, as well as measured 1-minute average 10 m wind speed and direction, are superimposed on the corresponding picture. Note that measured time trends in wind speed and direction can cause irregular plume shapes, e.g. for PRISMA and GHGSat C2, which are also cut off in these images due to plume length. Surface imagery from © Google Earth.

1.1. Quantification performance is similar to aircraft

For all detected emissions, mean estimates for all satellite-team combinations are accurate between -68% and 110% of the metered value (Figure 3; see also SI, Section S6), with 78% of

nonzero estimates falling within ±50% of the metered value. This performance is similar to error demonstrated by aerial remote sensing technologies, such as Kairos Aerospace, with 79% of nonzero single-blind estimates falling within ±50% of the metered value (described in detail in the SI, Section S5) [14] . See the SI, Section S6 for error summary statistics by satellite and team.

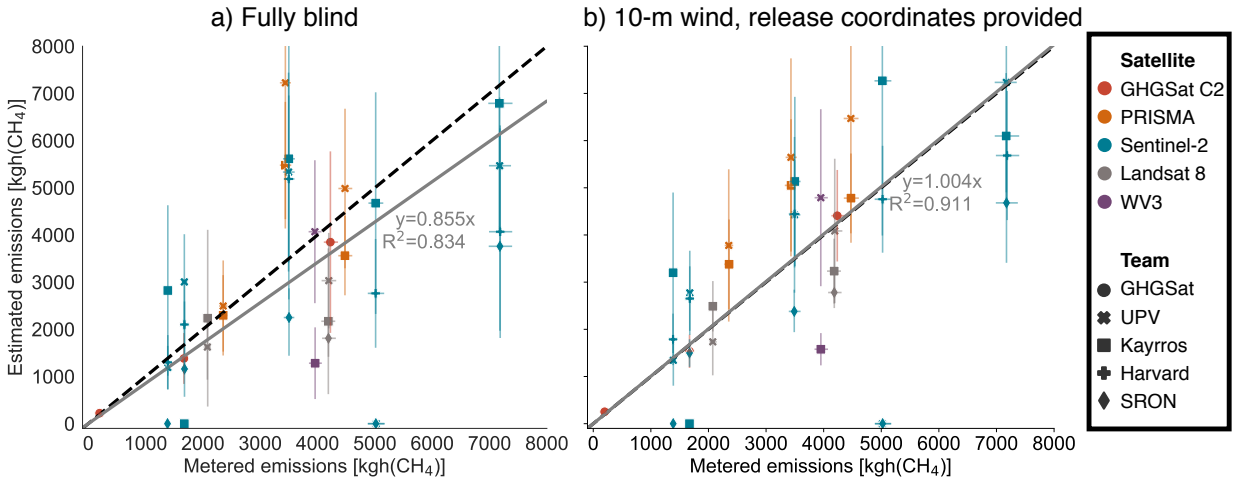

Figure 3. Quantification performance of methane emissions by satellite and team. Metered emissions compared with single-blind estimates for each overpass with successfully reported data, with 1-sigma X and Y error bars. a) Fully blind stage 1 results using modeled wind speed estimates. b) Stage 2 results using 10-m wind speed and direction measurements and the point source location of the plume. Percent error in both cases is similar to aircraft-based methane remote sensing methods. The grey solid line is a linear fit with the intercept fixed at zero, with slope and uncentered R^2 displayed. The black dashed line denotes perfect 1:1 agreement.

In stage 2 of the test, teams produced updated results using measured 10-m wind data from an on-site ultrasonic anemometer as well as precise coordinates of the single, stationary release location, though still blind to released volumes. These estimates are 20% higher on average than stage 1 estimates, roughly matching the average 19% underestimate in the modeled winds used in stage 1 (in emissions remote sensing methods, higher winds with the same observed methane enhancement imply greater methane flux). Applying an ordinary least squares linear fit to all quantified emissions, with the intercept set to zero, we see substantial improvement in slope, rising from 0.855 [0.715, 0.889] in stage 1 to 1.004 [0.889, 1.120] in stage 2, almost a perfect one-to-one average agreement, though still with substantial error (Figure 3). After incorporating on-site wind measurements the uncentered R^2 increases from 0.834 to 0.911, implying a tighter fit. Note that this fit treats each estimate from each team as an independent data point and that uncentered R^2 values from a linear fit with a zero intercept are not directly comparable to R^2 values from regressions with a nonzero intercept. See the SI, Section S6 for further detail.

Although errors for larger emissions decrease in stage 2, errors increase for some smaller emissions, resulting in a percent error distribution that is similar across stages, as shown in the SI, Section S6 alongside full regression results. These results highlight the likely importance of wind speed and emission source location as sources of uncertainty in current satellite-based methane quantification methods, alongside other algorithmic uncertainties.

Confidence intervals provided by teams appear to be slightly overconfident, with the metered value lying within 1-sigma error range 59% of the time, instead of the 67% one would expect for perfectly calibrated confidence intervals. Provided 95% confidence intervals, shown in the SI, Section S6 contain the true value 91% of the time. Note that this combines results from multiple teams and satellites. With a larger dataset, it will be possible to determine calibration for individual satellites and analysis teams, but this will require significant additional experimental work.

These results provide an approximate first upper bound for the minimum detection capabilities of each instrument. GHGSat detected the smallest emission of the campaign, at 0.197 [0.187, 0.208] t/h and maintained stage 1 error between -17% and 13% for each of the three measurements with valid data collection. See the SI, Section S6 for all quantification error summary statistics by satellite and team. Three of the four teams analyzing Sentinel-2 data detected the smallest emission, metered at 1.4 [1.3, 1.5] t/h, which is close to the expected minimum detection threshold of the method [5].

Discussion

How useful might these satellites be in detecting emissions for control and mitigation? Lauvaux et al. recently estimated that oil and natural gas emissions visible to the TROPOMI instrument, (detection limit of >10 t/h), represent 8-12% of estimated global emissions from the sector [8].

At present, the full distribution of methane emissions from oil and natural gas systems (or other methane-emitting industries) is not sufficiently characterized in most regions to determine the fraction of total regional emissions visible to satellites. We can, however, use data from the Chen, Sherwin et al. 2018-2020 comprehensive aerial survey of the New Mexico Permian Basin to simulate the capabilities of satellites in one high-emission basin, emitting an estimated 9.4% [5.9%, 12.7%] of total production [32]. A comprehensive survey of the same area of New Mexico over the same time period with wider-area satellites similar to Sentinel-2 or Landsat 8, with a minimum detection threshold of 1-5 t/h, would see 18-43% of total emissions estimated by Chen, Sherwin et al., from 11-117 individual detected emissions from over 30,000 oil and gas facilities [32]. A comprehensive survey with a sufficiently large network of point-and-shoot satellites with a minimum detection threshold of 0.1-0.5 t/h (such as GHGSat, PRISMA, or WorldView-3) would see an average of 55-81% of total estimated emissions, from 258-1182 individual detected emissions [32]. See the SI, Section S4 for the details of this regional survey simulation.

Importantly, improved technology is on the way. At least eight constellations with point source imaging capability are in orbit or scheduled for launch by the end of 2023 [12]. The constellation of satellites from Carbon Mapper has a designed detection limit of 0.05 - 0.15 t/h, with revisit times of 1-7 days at full constellation deployment [33]. If quantification accuracy is similar to what we observe in above real-world blind tests (especially at observed GHGsat accuracy), then we will be able to find and quantify a substantial fraction of global methane emissions from oil and gas and other point sources, anywhere on the planet, on daily-to-weekly scales. The complementary MethaneSAT project from the Environmental Defense Fund will provide independent coverage using another advanced purpose-designed methane sensor, with both point source and wide-area

methane flux estimation capabilities at somewhat larger spatial scales [34]. A total of eight area flux mapping satellites are scheduled for orbit by 2027 [12].

1.2. Toward a globally accepted methane satellite validation regime

It is increasingly clear that satellite-based detection efforts can play an important role in understanding methane emissions across borders. The adoption and acceptance of this approach will depend in part on the confidence all parties involved place in the technology itself. The five satellites we tested correctly detected most emissions and had no false positives, bolstering confidence in these techniques, at least in cases with a pre-identified potential emission source. Despite the need for larger plumes in order to obtain a signal (due to a comparatively large minimum detection threshold), the quantification accuracy is qualitatively similar to airplane-based technologies. Importantly, the only purpose-designed methane satellite we tested, GHGsat, achieved quantification accuracy better than +/- 20% in each of its studied plumes.

This study outlines a first step toward ongoing, operational blind testing of satellites quantifying methane point sources. Significantly more blind testing – like we performed above – is needed to ensure rapid uptake and trust. As the technology evolves, the validation task remains similar scientifically, but becomes increasingly important. Our test was conducted under near-ideal land surface and wind speed conditions, and teams were aware in advance of the approximate emission location. Rigorous characterization of the detection and quantification capabilities of airplane-based methane remote sensing systems requires of order 100 measurements, as in [14], more than 10 times the number for any satellite in this study. Achieving similar evaluation of existing and emerging satellites will thus require further data collection. Satellites are already providing invaluable insights into methane emissions from multiple industries [6,9]. Additional independent empirical validation under a range of field conditions will enable satellites to play an even greater role in reducing global methane emissions from oil and natural gas and industries including waste management, agriculture, and mining.

1. Data and code availability

All data and code required to reproduce the figures and analysis in this paper are available on GitHub at https://github.com/esherwin/SatelliteTesting.

2. Abbreviations

EPA	Environmental Protection Agency
GHG	Greenhouse gas
GSC2	GHGSat C2 (satellite)
LS8	Landsat 8
PRISMA	PRecursore IperSpettrale della Missione Applicativa
SI	Supplementary information
SRON	Stichting Ruimte Onderzoek Nederland
TROPOMI	TROPOspheric Monitoring Instrument
WV3	WorldView-3

3. Acknowledgments

We acknowledge Erin Tullos, Zhan Zhang, Christian Frankenberg, and ExxonMobil, particularly Felipe Javier Cardoso-Saldaña, for their thoughtful feedback. We received remote logistical support from participants Ryan Mattson, Quinn Chao, Rafael Del Bello, Marianne Girard, Jason McKeever, and Angel Esparza (GHGSat); Daniel Varon (Harvard); Sudhanshu Pandey (SRON); Alexandre d'Aspremont, Carlo de Franchis, Christian LeLong, and Clément Giron (Kayrros); and Elena Sánchez García, Itziar Irakulis Loitxate, Javier Gorroño Viñegla, and Luís Guanter (UPV). Rawhide Leasing provided indispensable operational, logistical, and planning support for the experiment.

4. Supplementary information available

Within this document.

5. Funding sources

This study was funded by ExxonMobil, the Stanford Strategic Energy Alliance, and the Stanford Natural Gas Initiative, an industry consortium that supports independent research at Stanford University.

6. Competing interests

E.A. Kort serves as unpaid chair for the Carbon Mapper science advisory panel, which is preparing a methane sensing satellite constellation for launch. The remaining authors have no competing interests to declare.

7. References

1. Kemp, C. E. & Ravikumar, A. P. New Technologies Can Cost Effectively Reduce Oil and Gas Methane Emissions, but Policies Will Require Careful Design to Establish Mitigation Equivalence. *Environ. Sci. Technol.* **55**, 9140–9149 (2021).
2. Tyner, D. R. & Johnson, M. R. A Techno-Economic Analysis of Methane Mitigation Potential from Reported Venting at Oil Production Sites in Alberta. *Environ. Sci. Technol.* **52**, 12877–12885 (2018).
3. CCAC. *Global Methane Pledge*. https://www.globalmethanepledge.org/ (2021).
4. Kort, E. A. *et al.* Four corners: The largest US methane anomaly viewed from space: Four Corners: largest US methane anomaly. *Geophys. Res. Lett.* **41**, 6898–6903 (2014).

5. Varon, D. J. *et al.* High-frequency monitoring of anomalous methane point sources with multispectral Sentinel-2 satellite observations. *Atmos. Meas. Tech.* **14**, 2771–2785 (2021).
6. Varon, D. J., Jacob, D. J., Jervis, D. & McKeever, J. Quantifying Time-Averaged Methane Emissions from Individual Coal Mine Vents with GHGSat-D Satellite Observations. *Environ. Sci. Technol.* **54**, 10246–10253 (2020).
7. Varon, D. J. *et al.* Satellite Discovery of Anomalously Large Methane Point Sources From Oil/Gas Production. *Geophys. Res. Lett.* **46**, 13507–13516 (2019).
8. Lauvaux, T. *et al.* Global Assessment of Oil and Gas Methane Ultra-Emitters. *Science* **375**, 557–561 (2022).
9. Irakulis-Loitxate, I. *et al.* Satellite-based survey of extreme methane emissions in the Permian basin. *Sci. Adv.* **7**, eabf4507 (2021).
10. CEOS. *A Constellation Architecture for Monitoring Carbon Dioxide and Methane from Space*. https://ceos.org/document_management/Virtual_Constellations/ACC/Documents/CEOS_AC-VC_GHG_White_Paper_Publication_Draft2_20181111.pdf (2018).
11. Irakulis-Loitxate, I., Gorroño, J., Zavala-Araiza, D. & Guanter, L. *Satellites detect a methane ultra-emission event from an offshore platform in the Gulf of Mexico*. http://eartharxiv.org/repository/view/3222/ (2022) doi:10.31223/X5504G.
12. Jacob, D. J. *et al. Quantifying methane emissions from the global scale down to point sources using satellite observations of atmospheric methane*. https://acp.copernicus.org/preprints/acp-2022-246/ (2022) doi:10.5194/acp-2022-246.
13. Ehret, T. *et al.* Global Tracking and Quantification of Oil and Gas Methane Emissions from Recurrent Sentinel-2 Imagery. *arXiv:2110.11832 [physics]* (2021).

14. Sherwin, E. D., Chen, Y., Ravikumar, A. P. & Brandt, A. R. Single-blind test of airplane-based hyperspectral methane detection via controlled releases. *Elementa: Science of the Anthropocene* **9**, 00063 (2021).
15. Ravikumar, A. P. *et al.* Single-blind Inter-comparison of Methane Detection Technologies - Results from the Stanford/EDF Mobile Monitoring Challenge. *Elementa: Science of the Anthropocene* **7**, 29 (2019).
16. Bell, C. S., Vaughn, T. & Zimmerle, D. Evaluation of next generation emission measurement technologies under repeatable test protocols. *Elementa: Science of the Anthropocene* **8**, 32 (2020).
17. Zimmerle, D. *METEC Controlled Test Protocol: Survey Emission Detection And Quantification*. https://mountainscholar.org/handle/10217/235363 (2022).
18. ESA. *About GHGSat*. https://earth.esa.int/eogateway/missions/ghgsat (2022).
19. Sánchez-García, E., Gorroño, J., Irakulis-Loitxate, I., Varon, D. J. & Guanter, L. *Mapping methane plumes at very high spatial resolution with the WorldView-3 satellite*. https://amt.copernicus.org/preprints/amt-2021-238/amt-2021-238.pdf (2021) doi:10.5194/amt-2021-238.
20. ESA. *Earth Online: Worldview-3*. https://earth.esa.int/eogateway/missions/worldview-3 (2022).
21. OHBI. *Satellites & Missions: PRISMA*. https://www.ohb-italia.it/satellites-missions/ (2022).
22. USGS. *Landsat 8*. https://www.usgs.gov/landsat-missions/landsat-8 (2022).
23. ESA. *Sentinel-2*. https://sentinel.esa.int/web/sentinel/missions/sentinel-2 (2021).
24. GHGSat. *Global leader in remote sensing of greenhouse gas*. https://www.ghgsat.com/en/who-we-are/ (2022).

25. Kayrros. *A partner for today and the future, agile with technology and with a smarter approach to data*. https://www.kayrros.com/who-are-we/ (2022).
26. Pandey, S. *et al.* Satellite observations reveal extreme methane leakage from a natural gas well blowout. *Proc. Natl. Acad. Sci. U.S.A.* **116**, 26376–26381 (2019).
27. Sadavarte, P. *et al.* Methane Emissions from Superemitting Coal Mines in Australia Quantified Using TROPOMI Satellite Observations. *Environ. Sci. Technol.* **55**, 16573–16580 (2021).
28. Irakulis-Loitxate, I., Guanter, L., Maasakkers, J. D., Zavala-Araiza, D. & Aben, I. Satellites Detect Abatable Super-Emissions in One of the World's Largest Methane Hotspot Regions. *Environ. Sci. Technol.* **56**, 2143–2152 (2022).
29. Irakulis-Loitxate, I. *et al.* Satellite-based survey of extreme methane emissions in the Permian basin. *Sci. Adv.* **7**, eabf4507 (2021).
30. Guanter, L. *et al. Mapping methane point emissions with the PRISMA spaceborne imaging spectrometer*. http://eartharxiv.org/repository/view/2344/ (2021) doi:10.31223/X5VC9C.
31. Varon, D. J. *et al.* Quantifying methane point sources from fine-scale satellite observations of atmospheric methane plumes. *Atmos. Meas. Tech.* **11**, 5673–5686 (2018).
32. Chen, Y. *et al.* Quantifying Regional Methane Emissions in the New Mexico Permian Basin with a Comprehensive Aerial Survey. *Environmental Science & Technology* 7.
33. CarbonMapper. *Carbon Mapper: Accelerating local climate action, globally*. https://carbonmapper.org/ (2022).
34. MethaneSAT. *New Satellites Unlock Crucial Climate Opportunity*. https://www.methanesat.org/fit-with-other-missions/ (2022).

35. *QuadraTherm® 640i/780i Series Insertion and In-Line Mass Flow Meters Instruction Manual*. https://www.sierrainstruments.com/userfiles/file/manuals/640i-780i-instruction-manual.pdf?x=5063 (2020).
36. Rutherford, J. S., Sherwin, E. D., Chen, Y. & Brandt, A. R. *Controlled release experimental methods: 2021 Stanford controlled releases in TX and AZ*. https://eao.stanford.edu/sites/g/files/sbiybj22256/files/media/file/Method_description_Setup_and_Uncertainty_v18.pdf (2022).
37. GPSA. Section 1 General Information. in *Engineering Data Book* vol. 1 (Gas Processors Supply Association, 2011).
38. ESA. *Sentinel-5P: Global AIr Monitoring for Copernicus*. https://esamultimedia.esa.int/docs/EarthObservation/Sentinel-5p_factsheet_171211.pdf (2022).
39. ESA. *GHGSat data now available through ESA's Earthnet programme*. https://earth.esa.int/eogateway/news/ghgsat-data-now-available-through-esa-s-earthnet-programme (2021).
40. ESA. *WorldView-3 full archive and tasking*. https://earth.esa.int/eogateway/catalog/worldview-3-full-archive-and-tasking (2022).
41. USGS. *Landsat Data Access*. https://www.usgs.gov/landsat-missions/landsat-data-access (2022).
42. ESA. *Sentinel-2: About the launch*. https://www.esa.int/Applications/Observing_the_Earth/Copernicus/Sentinel-2/About_the_launch.

43. ESA. *Sentinel-2 User Handbook*. 64 https://sentinel.esa.int/documents/247904/685211/Sentinel-2_User_Handbook (2015).
44. ESA. *Access to Sentinel data via download*. https://sentinel.esa.int/web/sentinel/sentinel-data-access (2021).
45. ESA. *Sentinel-5P*. https://sentinel.esa.int/web/sentinel/missions/sentinel-5p (2021).
46. ESA. *Sentinel Online: Geographical Coverage*. https://sentinel.esa.int/web/sentinel/missions/sentinel-5p/geographical-coverage (2021).
47. ESA. *Sentinel Online: Instrumental Payload*. https://sentinel.esa.int/web/sentinel/missions/sentinel-5p/instrumental-payload (2021).
48. Gordon, I. E. *et al.* The HITRAN2020 molecular spectroscopic database. *Journal of Quantitative Spectroscopy and Radiative Transfer* **277**, 107949 (2022).
49. Kneizys, F. X. *et al. User guide to LOWTRAN 7*. 147 (1988).
50. Frankenberg, C. *et al.* Airborne methane remote measurements reveal heavy-tail flux distribution in Four Corners region. *Proc Natl Acad Sci USA* **113**, 9734–9739 (2016).

Supplementary information for "Testing satellite-based methane sensing: Single-blind validation strengthens international methane regulation"

Authors: Evan D. Sherwin[1,*], Jeffrey S. Rutherford[1], Yuanlei Chen[1], Sam Aminfard[2], Eric A. Kort[3], Robert B. Jackson[4], Adam R. Brandt[1]

Author Affiliations:

[1] Department of Energy Resources Engineering, Stanford University, Stanford, California 94305, United States

[2] ExxonMobil Upstream Research Company, Spring, Texas 77389, United States

[3] Climate and Space Sciences and Engineering, University of Michigan, Ann Arbor, Michigan 48109, United States

[4] Earth System Science, Woods Institute for the Environment and Precourt Institute for Energy, Stanford University, Stanford, California 94305, United States

[*] Correspondence: evands@stanford.edu

Table of contents

S1 Materials and Methods

S1.1 Materials

For the duration of testing, our controlled methane releases apparatus was located near Ehrenberg, Arizona, on the border of Arizona and California, at approximately [33.630637°, -114.487755°]. These are the coordinates initially given to all satellite operators.

The methane source was a trailer of liquefied natural gas, shown in Figure 4, which was reheated from roughly -160° C to temperatures generally ranging from 30-65° C, within the rated tolerance of our Sierra QuadraTherm 640i meters [35]. For the October 19 Sentinel-2 overpass, a heater issue resulted in a gas temperature of -38°C, still within range but close to the minimum rated temperature of -40°C. The gas was then transmitted to the metering and release trailer via an 8" shipping hose at an exit pressure of roughly 80-150 psi (0.55-1 Mpa), passing through one of four possible metering locations before release through a single release stack located at [33.630645°, -114.489150°], at a release height of 5 m above ground level, shown in Figure 5.

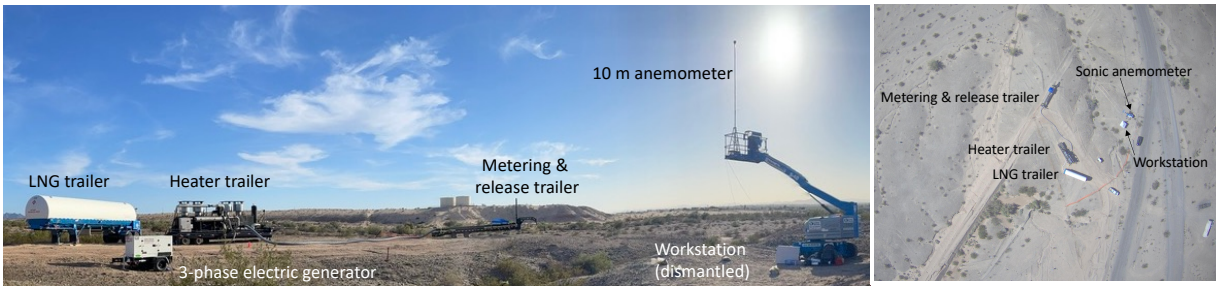

Figure 4. The experimental setup in panorama (left). Liquefied natural gas was reheated before flowing through a metering and release trailer. An aerial photograph of the site (right) [courtesy of Bridger Photonics Inc.]. Note that the release trailer is ~45 m from LNG trailer and ~45 m from workstation and anemometer. Adapted with permission from [36].

Figure 5. Metering and release trailer (left) has four pipes (0.5-inch, 2-inch, 4-inch, and 8-inch), each leading to a distinct metering location allowing a different dynamic range of release volumes. The three larger pipes used a QuadraTherm 640i insertion meter (right), with upstream 8.5 m straight run of pipe to ensure sufficient flow stabilization for all pipes. The 0.5-inch pipe was not used in this study.

This experiment used only the 2-inch, 4-inch and 8-inch pipes to achieve the desired release volumes. Using QuadraTherm 640i insertion meters, the maximum achievable release rate for the 8-inch pipe is 416,400 standard cubic feet per hour (scfh), or 8.0 t/h for pure methane. For the 4-inch pipe, the maximum release rate is 106,080 scfh or 2.0 t/h for pure methane, falling to 27,960 scfh or 0.5 t/h for the 2-inch pipe [37]. These values fall by roughly 20% for the meter used for the November 3 Sentinel-2 release. See [36] for further detail.

S1.2 Safety

All natural gas equipment fabrication, transportation, assembly, and operation was conducted by personnel from Rawhide Leasing, a gas services contractor. No Stanford personnel operated natural gas release equipment. The research workstation, at which Stanford researchers coordinated field operations and data collection procedures, was ~45 m away from all equipment through which natural gas flowed and researchers maintained a distance of at least 30 m from this equipment during active releases.

In addition, Stanford researchers continuously monitored plume dissipation in real time using a FLIR infrared camera and paid continuous attention to olfactory signals from the odorized gas. The infrared camera showed clear plume dissipation well before reaching any on-site personnel, particularly because the emission source was elevated and gas often exited at a high vertical velocity, accelerating natural methane lofting. Stanford researchers rarely detected gas by smell during the test period.

S1.3 Data logging

Stanford researchers logged data from the gas flow meters using a Eurotherm Nanodac automatic data logger, with an iPhone-based Zoom livestream of the digital meter display as a backup. All data in this study use the automatic data logger except the GHGSat and PRISMA measurements on October 16 and the Landsat 8 measurements on October 21, which use Google optical character recognition to extract a flow rate time series from the Zoom livestream. Data from the data logger and the Zoom livestream of the digital meter display agree to within 1%.

S1.4 Data collection procedures

All satellite-coincident releases began at least 15 minutes before the scheduled satellite overpass time, provided by participating teams. Initial releases began as much as 30 minutes in advance. After receiving initial plume images from satellite participants, it became clear that a methane plume moving at the average wind speed would stabilize well within 15 minutes at the release volumes in this study. In practice, all emission rates stabilized within 11 minutes of the satellite overpass.

A Rawhide Leasing technician set all release levels based on hand signals from the Stanford team, which requested adjustments to release volumes based on the Zoom livestream of the digital meter readout. Due to the engineering properties of the gas release system, flow rates often varied somewhat during these releases. Stanford personnel aimed to maintain rates within ±10% of the targeted value and requested adjustments as needed from Rawhide Leasing personnel.

S1.5 Flow rate uncertainty

Sources of uncertainty in measured flow rates include variability in actual flow rates (captured as the standard deviation of metered flow over a 5-minute period), rated meter uncertainty, error introduced by variation in meter placement during installation, and uncertainty in gas composition, which can vary even for a consistent supplier. We propagate these sources of error into our metered values using a Monte Carlo-based approach with 10,000 iterations. See [36] for further discussion of sources of metering uncertainty and the Monte Carlo approach.

The 5-minute averaging period used to compute flow variability is based on the fact that a plume traveling with a relatively slow average wind speed of 2 m/s would traverse 600 m within 5 minutes (300 seconds). By this distance, much of the originally emitted methane has likely dissipated into background concentrations, with the bulk of the methane enhancement detected by a satellite remaining closer to the release point. A sensitivity analysis in

shows that switching this averaging period to 60 seconds or 600 seconds has a minimal effect on the results.

S1.6 Experimental design

This single-blind field trial employed a two-stage experimental design,

Stanford personnel initially released metered quantities of methane from the Arizona test site via procedures described above and in [36]. The Stanford ground team and contract personnel operating equipment communicated no information to participating teams regarding metered flow rates, metered wind speed or direction, or the precise location of ground-based equipment. In addition, participating teams were not informed of the details of the equipment or its configuration, e.g. the use of liquefied natural gas v. compressed natural gas (which Stanford used in previous tests), or the diameter of the pipes and hoses involved.

Thus, all teams produced stage 1 estimates using only information from their existing systems, including the satellites and available wind reanalysis products, based on coordinates that identified the release location to within 0.65 km.

After each team submitted finalized stage 1 estimates, we provided 10 m wind speed and direction readings from our on-site ultrasonic anemometer, as well as the precise coordinates of the release stack, [33.630645°, -114.489150°]. All teams submitted both stage 1 and stage 2 estimates on a timeline described below in Table 2. Note that turnaround time in these tests may not be representative of field performance.

Table 2. Data submission timeline by stage for each team.

Operator	Submitted Stage 1	Received Wind and Location Data	Submitted Stage 2
GHGSat	1-Dec-21	8-Dec-21	28-Feb-22
Kayrros	26-Nov-21	13-Jan-22	28-Feb-22
Valencia	11-Nov-21	11-Feb-22	23-Feb-22
SRON	25-Feb-22	25-Feb-22	28-Feb-22
Harvard	2-Feb-22	23-Feb-22	25-Feb-22

S2 Participating satellites

Six satellites commonly used for methane sensing were available to collect measurements during the study period of October 16-November 3, 2021. This included targeted satellites GHGSat, WorldView-3, and PRISMA, which must be tasked to focus on a particular area, as well as global-coverage satellites Landsat-8, Sentinel-2, and Sentinel-5P (TROPOMI), which passively collect data from nearly all inhabited areas of the world [18,20–23,38].

Table 1 summarizes the spectral resolution, spatial coverage, constellation size, swath width, revisit time, and data availability (commercial or public). We opted not to test Sentinel-5P due to its lower resolution, which corresponds to a minimum methane detection limit likely above the capabilities of our equipment. Below, we describe each satellite in more detail.

Note that only the GHGSat instruments were originally designed for the primary purpose of detecting and quantifying methane emissions. With the remaining satellites, researchers have developed methane retrieval techniques based on existing data [5,8,9,28].

S2.1 GHGSat-C2

The GHGSat-C2 satellite is one of two instruments launched by the Canada-based private company GHGSat. GHGSat-C2 was launched on January 24, 2021, following the launch of its counterpart, GHGSat-C1, On September 2, 2020. The precursor GHGSat-D satellite was launched on June 22, 2016. Several additional satellites are scheduled to launch in the coming years, with contracts awarded for GHGSat-C3, -C4, and -C5, with a goal of achieving a 10-satellite constellation by 2023 [18].

GHGSat C1 and C2 each complete 15 orbits per day, with a 14-day repeat cycle. Each satellite is equipped with a multispectral Wide-Angle Fabry-Perot (WAF-P) Imaging Spectrometer, focusing on a proprietary combination of unpolarized short-wave infrared frequencies from 1630-1675 nm at 25m spatial resolution, as well as a secondary VIS-1 Visible Sensor in the optical frequency range at <20m spatial resolution. The sensor has a 12x12 km field-of-view, which can be targeted toward a desired location. GHGSat claims a detection threshold of 100 kg(CH4)/h at 3 m/s winds, with methane column density precision at 1% of background [18].

GHGSat operates commercially, but offers access to data archives as well as tasking to scientific researchers for select proposals [39].

S2.2 WorldView-3

Launched August 13, 2014, the WorldView-3 satellite is owned and operated by United States-based company Maxar. This multispectral instrument measures in one panchromatic band, eight multispectral bands in the visible near infrared range, eight short-wave infrared (SWIR) bands, and 1195-2365 nm, and twelve bands covering clouds, aerosols, vapors, ice, and snow. This targeted instrument has an 13.1 km swath and a revisit frequency of 4.5 days at 20° off-nadir for maximum resolution [20].

WorldView-3 operates commercially, its data archives as well as tasking are available to scientific researchers for select proposals [40].

S2.3 PRISMA

Launched March 19, 2019, the PRISMA (PRecursore IperSpettrale della Missione Applicativa) satellite is a product of the Italian Space Agency (ASI), contracting through Orbitale Hochtechnologie Bremen (OHB) Italia S.p.A. This targeted hyperspectral instrument uses spectral bands ranging from 400-2,500 nm with a 30 km swath, operating with a 7-day maximum revisit frequency. Data from PRISMA are publicly available, and the satellite can be tasked upon request [21].

S2.4 Landsat 8

Launched on February 11, 2013, the Landsat 8 satellite is the product of a collaboration between the National Aeronautics and Space Administration (NASA) and the United States Geological Survey (USGS), both agencies of the United States government. This instrument has global coverage, collecting data for all inhabited areas of the world every 16 days with an 185 km swath. The satellite hosts a 9-band operational land imager, including two SWIR bands at 1570-1650 nm and 2110-2290 nm, as well as four visible bands, all at 30 m resolution. An onboard thermal infrared sensor also collects two bands at 10,600-11,190 nm and 11,500-12,510 nm, both at 100 m resolution. All data from Landsat 8 are publicly available at [41].

S2.5 Sentinel-2

The two-satellite Sentinel-2 constellation consists of Sentinel 2A, launched June 23, 2015, and Sentinel 2B, launched March 7, 2017 as part of the European Union's Copernicus program [42]. The satellites operate in the same 10-day polar orbit offset by 180°, resulting in 5-day revisit times at the equator, falling to 2-3 days at mid-latitudes. Each satellites collects data for all inhabited areas of the world each orbit with 290km swath with thirteen spectral bands in the SWIR and Visible to Near Infrared ranges. This includes four bands at 10 m resolution, six bands at 20m resolution (including Band 12 at 2190 nm in the SWIR range), and three bands at 60m resolution [43]. All data from Sentinel-2 are publicly available at [44].

S2.6 Sentinel-5P (TROPOMI)

The Sentinel-5 Precursor (Sentinel-5P) satellite was launched October 13, 2017, also as part of the European Union's Copernicus program [45]. This satellite offers full daily coverage for latitudes greater than 7° or less than -7° and over 95% coverage for remaining latitudes, with a 2600 km swath and 7 km pixels [46]. The onboard TROPOspheric Monitoring Instrument (TROPOMI) includes four spectrometers, each with two spectral bands, including two the ultraviolet, two in the visible range, two in the near infrared, and two SWIR bands [47]. All data from Sentinel-5P are publicly available at [44]. Due to the low spatial resolution of the instrument, its estimated methane detection threshold is approximately 10 t(CH4)/h, too large to test with our equipment in this study [8].

S3 Participating teams

Five teams participated in this single-blind study, each using data from a subset of the five participating satellites.

We invited all teams of which we were aware that estimate methane emissions from any of the five participating satellites.

Each team was given the option to produce methane retrievals for up to five participating satellites. GHGSat was the only company with access to data from GHGSat C2 and was thus the only team able to produce an estimate from that satellite, as shown in Table S1.

Table S1. Satellites (columns) analyzed by each team (rows). The final column is the reported source for 10 m wind data for fully blind estimates.

Team	GHGSat C2	Landsat-8	PRISMA	Sentinel-2	WorldView-3	Wind source
GHGSat	X					GEOS-FP
Kayrros		X	X	X	X	ECMWF ERA5
SRON		X		X		ECMWF ERA5, GEOS-FP
UP Valencia		X	X	X	X	GEOS-FP
Harvard				X		GEOS-FP

In fully blind stage 1 estimates, all teams used wind reanalysis data from either NASA Goddard Earth Observing System-Fast Processing (NASA GEOS-FP) at 10 m, Fifth generation European Centre for Medium-Range Weather Forecasts Atmospheric Reanalysis of the global climate (ECMWF ERA5), or both (*1*, *2*).

S3.1 GHGSat

GHGSat is a private company specializing in remote sensing of greenhouse gas emissions. GHGSat owns a constellation of satellites, currently including GHGSat D as well as the more recent GHGSat C1 and C2 instruments, with further satellites scheduled for launch in coming years [10]. GHGSat also produces estimates of methane emissions from other satellites, including Sentinel-2, but opted not to do so for this study, in part due to time constraints as the Stanford team did not realize this possibility until one month before the unblinding deadline.

Firmware installed on the GHGSat C2 instrument was version 10.9.3-gb41c76f, using observation script N08AEB15.GSB. Methane retrievals were then conducted using toolchain version 8.23, via the ghg-ops-srr v0.9.1 Source rate retrieval algorithm. See the "Performer Info" tab of the GHGSat reported data spreadsheet for further detail.

S3.2 Kayrros

Kayrros is a private company specializing in reanalysis of public and private satellite data, with a major area of focus in remote sensing of methane. Kayrros produced estimates for all satellites except GHGSat C2.

Kayrros retrievals for all satellites relied on methods derived from the algorithm introduced in Varon et al. 2018 [31], the molecular spectroscopic database introduced in the HITRAN2020 model [48], and the LOWTRAN 7 atmospheric transmittance and background radiance model [49]. See the "Performer Info" tab of the Kayrros reported data spreadsheets for further detail.

S3.3 Stichting Ruimte Onderzoek Nederland (SRON)

SRON is the Dutch government space agency, which has a significant focus on remote sensing of methane emissions. Dr. Sudhanshu Pandey produced estimates for Sentinel-2 and LandSat 8 on behalf of SRON.

SRON retrievals relied on the multi-band–multi-pass integrated mass enhancement methane retrieval method introduced in Varon et al. 2021 [5]. See the "Performer Info" tab of the SRON reported data spreadsheets for further detail.

S3.4 Universitat Politècnica de València

Researchers Prof. Luís Guanter, Itziar Irakulis Loitxate, and Javier Gorroño Viñegla of Universitat Politècnica de València (UPV) in Spain produced estimates for all satellites except GHGSat C2.

UPV researchers did not report the details of their retrieval algorithms in this study but did so in other studies. Irakulis-Loitxate et al. used a matched filter-based method for PRISMA retrievals in [29], and for Sentinel-2 and Landsat 8 retrievals in [28]. Sánchez-García et al. [19] apply a retrieval method derived from Frankenberg et al. 2016 and Varon et al. 2018 [31,50] to estimate methane emission rates using WorldView-3.

S3.5 Harvard University

Dr. Daniel Varon of Harvard University developed the first method for estimating methane emissions from Sentinel-2 data [5]. Dr. Varon produced estimates for Sentinel-2 only.

Dr. Varon used a modified version of the algorithm described in Varon et al. 2021 [5], adding concepts from Ehret et al. 2021 [13]. See the "Performer Info" tab of the Harvard reported data spreadsheet for further detail.

S4 Determining what satellites would see in the New Mexico Permian Basin

To estimate total methane emissions that a satellite with a given minimum detection limit, γ, would see in the field, we use a dataset of emissions detected during a comprehensive aerial survey of the New Mexico Permian Basin [32]. We compute total emissions from the survey with reported magnitude greater than or equal to γ and divide this sum by 4, the average number of times each asset was visited, to compute a rough persistence-averaged regional emissions estimate. Note that the survey covered only ~90% of assets in the region and emissions estimates computed this way do not account for emissions from the ~10% of uncovered assets [32]. Thus the total emissions estimates produced from this analysis are likely conservative.

S5 Estimating the fraction of Kairos controlled releases with error <±50%

We use the results of controlled release testing from [14] to compute the fraction of Kairos estimates that fell within ±50 of metered values. As in the paper, we assume natural gas is 93.5% methane (based on local gas composition reports from the utility from which we purchased the natural gas) and use wind speeds measured from the cup wind meter, which was present for all measurements [14].

S6 Supplementary results

Supplementary regression results

To estimate the overall quantification accuracy, goodness of fit, and error distribution of all quantified methane emission estimates, we apply a linear regression. Due to the relatively small sample size, large scatter, and relative absence of metered emission rates below 1 t/hr, a traditional ordinary least squares linear fit with a nonzero y-intercept yields an artificially high intercept (stage 1: 1.3 [0.1, 2.4] t/hr, stage 2: 1.1 [0.2, 2.1] t/hr) and an artificially low slope (0.577 [0.290, 0.864], stage 2: 0.7497 [0.518, 0.982]). We correct for this artifact of the data structure by fixing the y-intercept at zero in the regression, shown in Eq. (1).

$$y = \beta x \quad (1)$$

Where x is the mean metered emission rate, and y is the central emissions estimate provided by participating teams. These x and y values correspond to the markers in Figure 3.

The regression only includes quantified emissions, and does not include emissions that were not detected. We do this to assess the error distribution of detected emissions.

Table 2. Regression results for stages 1 and 2 based on the fixed-intercept ordinary least squares regression in Eq. (1).

	Stage 1	Stage 2
β	0.855 [0.715, 0.889]	1.0043 [0.889, 1.120]
Standard error	0.069	0.057
t-statistic	12.474	17.761
No. Observations	32	32
Degrees of freedom (Residuals)	31	31
Degrees of freedom (Model)	1	1
R^2	0.834	0.911
Adjusted R^2	0.829	0.908
F-statistic	155.6	315.4

R^2 values are presented in uncentered format due to the absence of a y-intercept term in the regression specification. As a result, these R^2 values are not directly comparable with the centered R^2 values produced in regressions with a y-intercept.

Note that these regressions treat each estimate from each team and satellite as independent and identically distributed observations. This aggregation is necessary to produce a meaningful regression due to the small sample size for each satellite and team, but the results of this analysis should be treated as a rough illustration of the general capabilities of the participating satellites and teams as a whole. Detailed characterization of the quantification accuracy from individual satellites and teams will require more data points.

Error statistics by satellite and team

Table 3. Summary statistics of quantified (non-zero) emissions by satellite, across all team.

		Stage 1				Stage 2			
	Count	Min	Mean	Max	σ	Min	Mean	Max	σ
GHGSat C2	3	-17%	-4%	13%	16%	-8%	8%	28%	18%
Landsat 8	5	-57%	-29%	7%	25%	-34%	-11%	20%	21%
PRISMA	6	-20%	27%	110%	49%	7%	44%	64%	20%
Sentinel-2	16	-48%	7%	103%	48%	-35%	19%	131%	43%
WV3	2	-68%	-32%	3%	50%	-60%	-19%	21%	58%

Table 4. Summary statistics of quantified (non-zero) emissions by team, across all satellites.

		Stage 1				Stage 2			
	Count	Min	Mean	Max	σ	Min	Mean	Max	σ
GHGSat	3	-17%	-4%	13%	16%	-8%	8%	28%	18%
Harvard	5	-45%	-4%	48%	41%	-21%	18%	58%	31%
Kayrros	10	-68%	8%	103%	52%	-60%	24%	131%	52%
SRON	4	-57%	-43%	-31%	12%	-35%	-28%	-10%	12%
UPV	10	-28%	17%	110%	48%	-16%	26%	65%	31%

Aggregate error statistics and effect of metered time averaging period

Table 5. Summary statistics of the percent error of estimated emission rates, as well as stage 1 wind speed error. Compares central estimates with 5-minute mean measured emissions. Note that although the standard deviation of the percent error distribution falls slightly after wind unblinding in stage 2, the inter-quartile range between the 25th and 75th percentiles of the error distribution is larger in stage 2. Thus, although by some metrics the linear fit improves using 10-m wind measurements, doing so in this case leads to larger percent errors for some smaller emission rates, leading to a similar overall percent error distribution. Note that the stage 1 percent error distribution does not change appreciably if the 300-second time average is replaced with 60 seconds or 600 seconds.

Metric	**Stage 1 (fully blind)**	**Stage 2 (measured wind)**	**Wind speed**	**Stage 1 (60s meter avg)**	**Stage 1 (600s meter avg)**
Mean	2%	16%	-19%	2%	2%
Standard deviation	45%	39%	25%	46%	45%
Min	-68%	-60%	-52%	-67%	-68%
P25	-28%	-12%	-39%	-28%	-29%
P50 (median)	-7%	13%	-22%	-8%	-6%
P75	16%	45%	-3%	17%	17%
Max	111%	130%	60%	113%	108%
Inter-quartile range (P75-P25)	45%	57%	35%	45%	46%

Detection summary

Table 6. Detection results by satellite and team. A tabular representation of Figure 1.

Satellite	Team	# True positive	# False negative	# True negative	# false positive	# Filtered retrieval	# Not tasked
GHGSat C2	GHGSat	3	0	0	0	0	2
Landsat 8	UPV	2	0	0	0	0	0
Landsat 8	Kayrros	2	0	0	0	0	0
Landsat 8	SRON	1	0	0	0	1	0
PRISMA	UPV	3	0	0	0	0	1
PRISMA	Kayrros	3	0	0	0	0	1
Sentinel-2	UPV	4	1	1	0	1	0
Sentinel-2	Kayrros	4	1	1	0	1	0
Sentinel-2	SRON	3	2	0	0	2	0
Sentinel-2	Harvard	5	0	1	0	1	0
WV3	UPV	1	0	0	0	0	0
WV3	Kayrros	1	0	0	0	0	0

Table 7. Ground truth for detection by satellite. Includes the count of non-zero emissions as well as zero-emission controls given to each satellite for all measurements (all instances in which the satellite passed overhead).

Satellite	# Non-zero	# Zero
GHGSat C2	5	0
Landsat 8	2	0
PRISMA	4	0
Sentinel-2	6	1
WV3	1	0

Supplementary figures

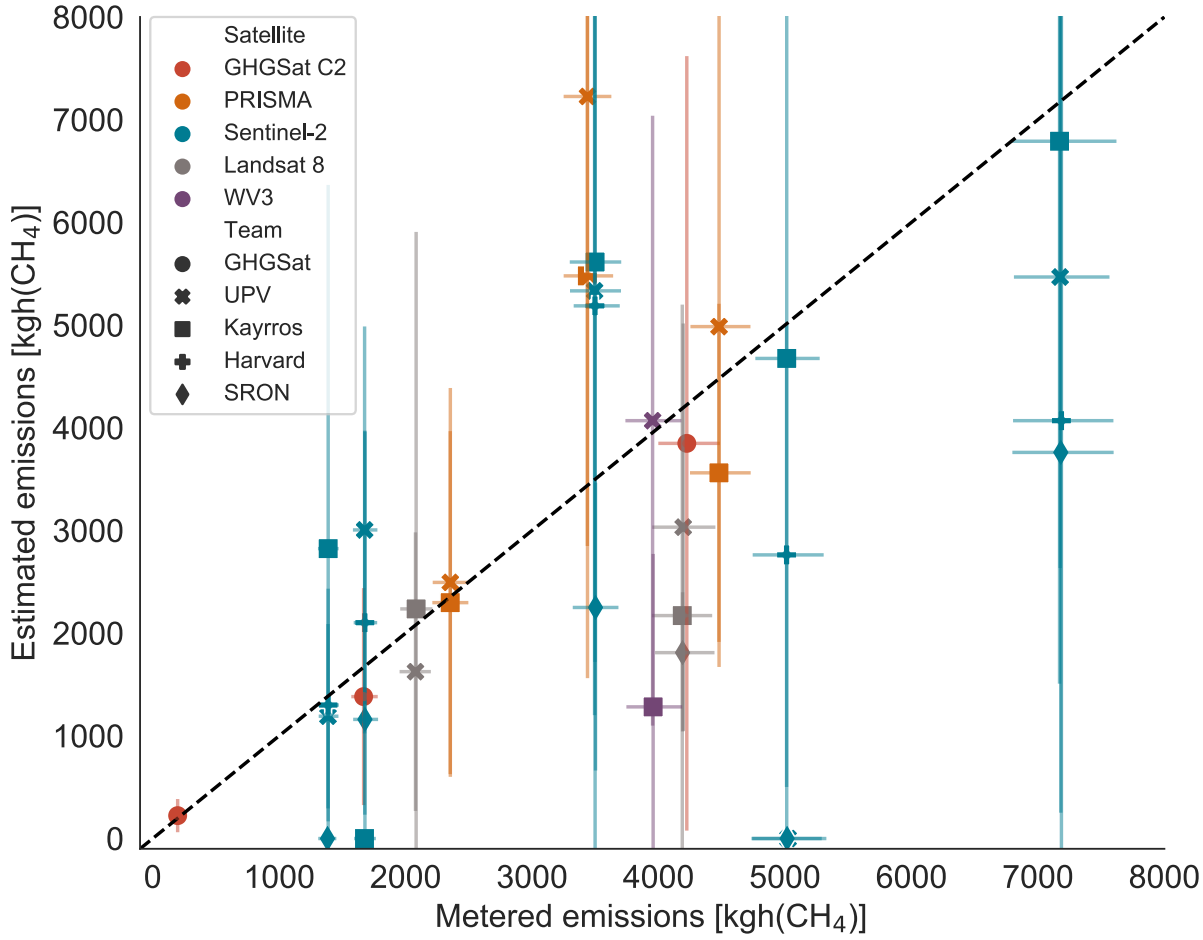

Figure 6. Stage 1 quantification estimates (fully blind) with 95% confidence intervals.

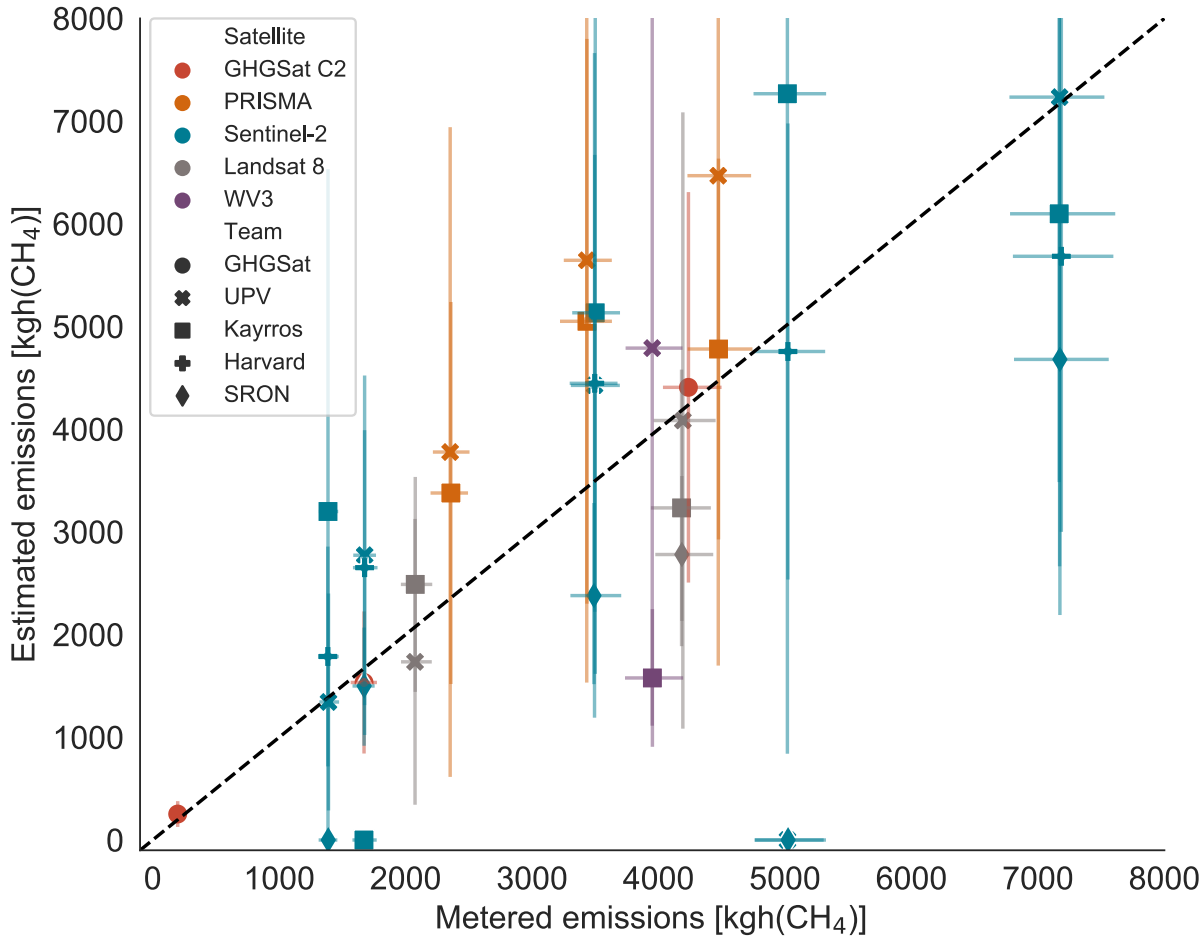

Figure 7. Stage 2 quantification estimates (with measured 10-m wind speed and direction as well as the precise coordinates of the release point) with 95% confidence intervals.

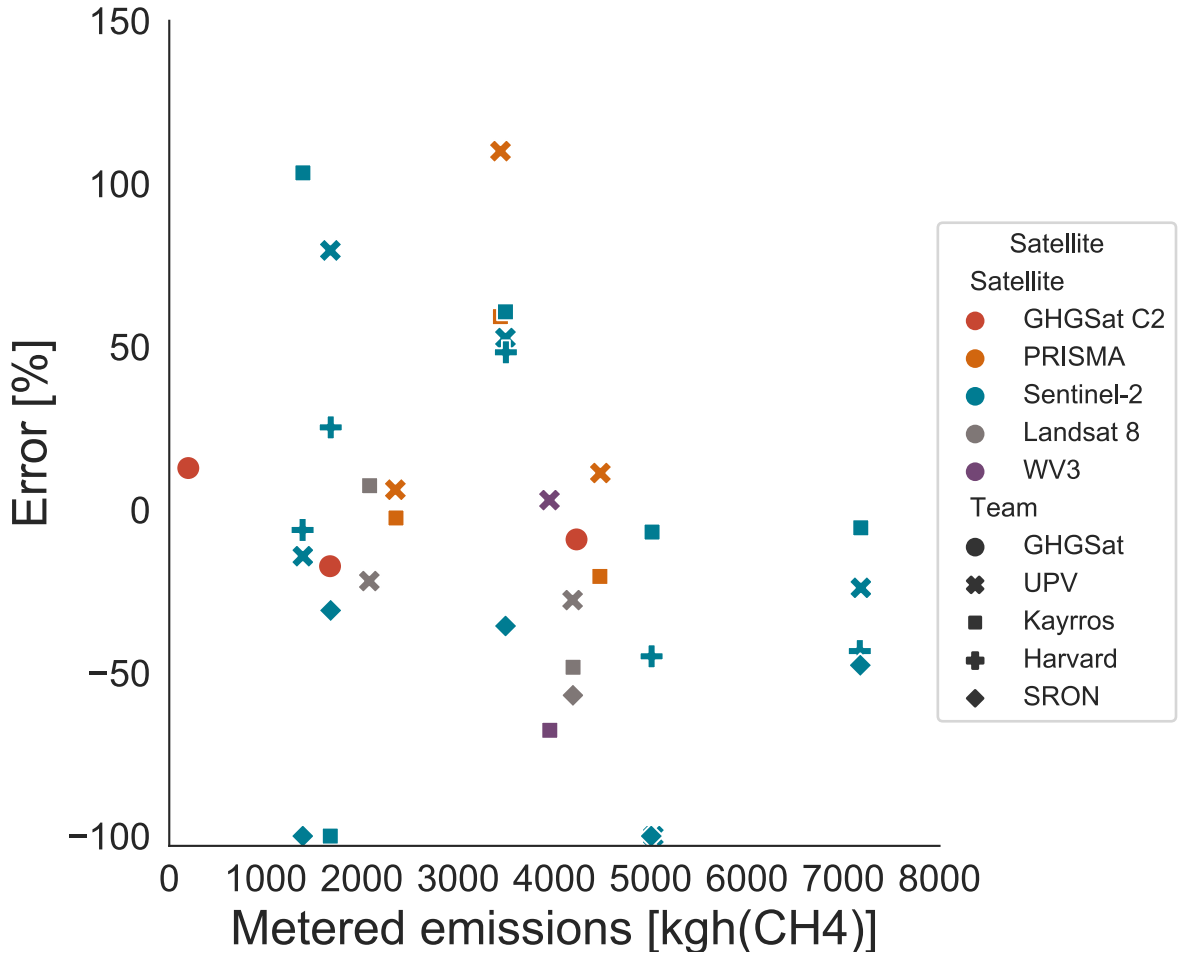

Figure 30. Stage 1 percent error for each mean quantification estimate.

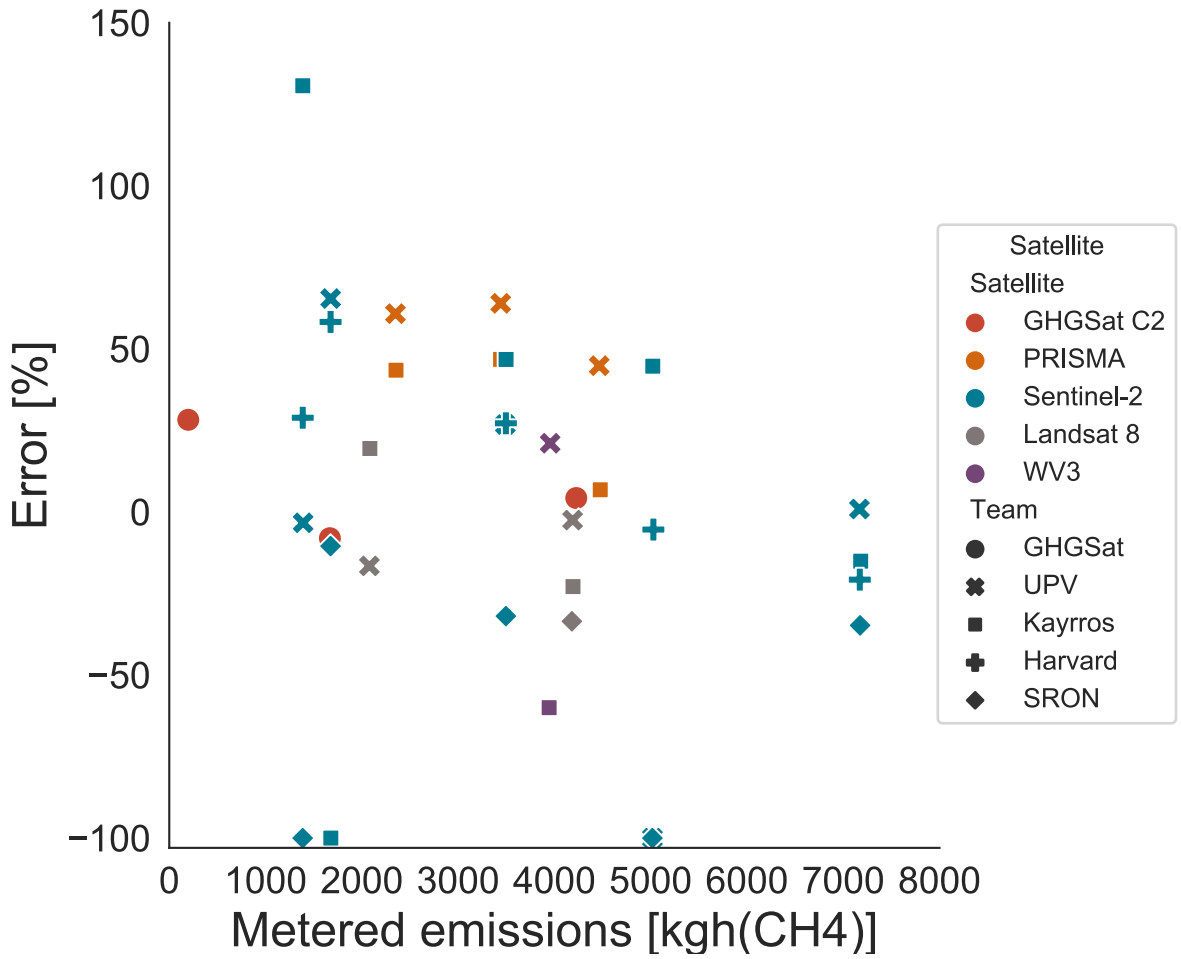

Figure 31. Stage 2 percent error for each mean quantification estimate, with 10 m wind data from an on-site ultrasonic anemometer as well as precise coordinates for the release location.

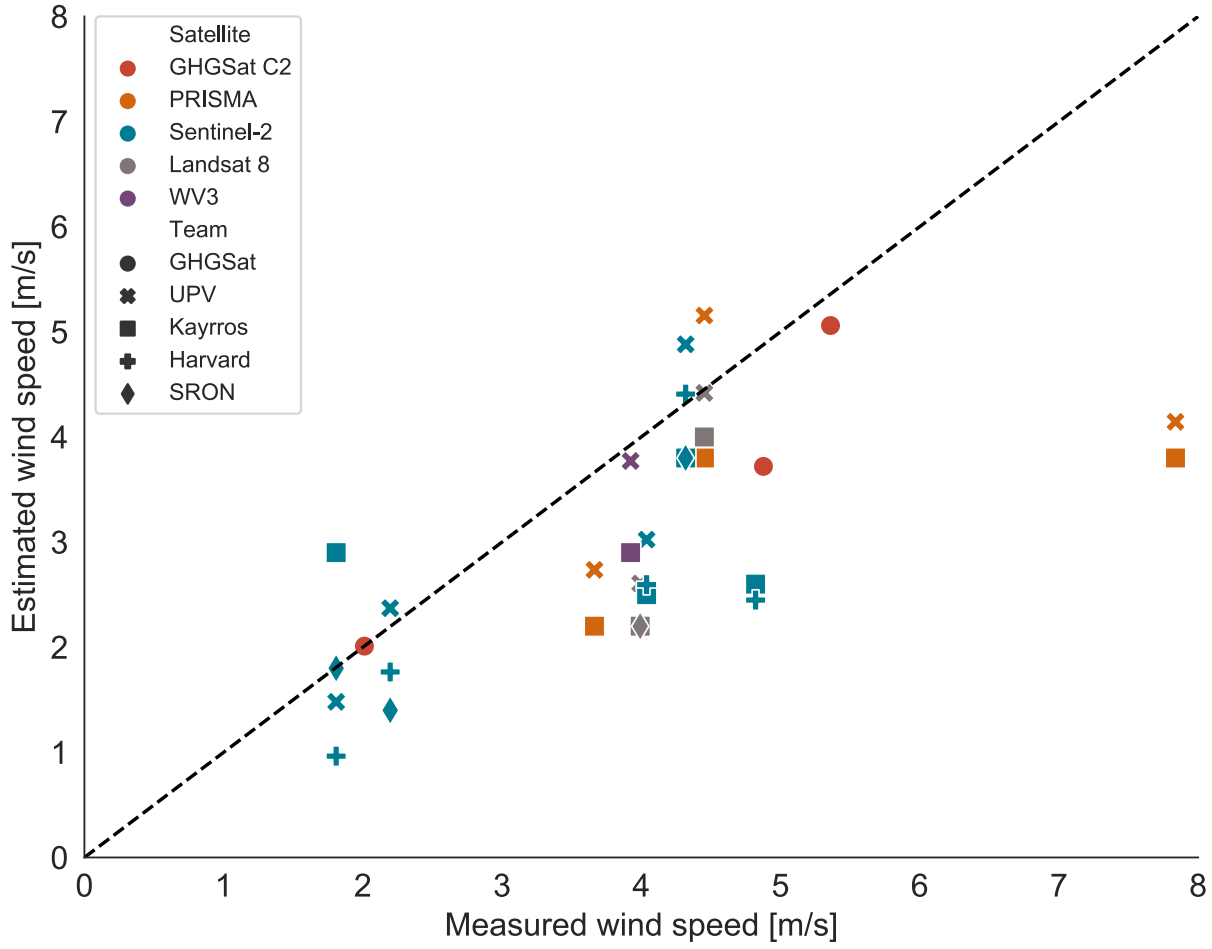

Figure 8. Parity chart of wind speed estimates used by teams in Stage 1 compared with 1-minute averages from the 10-m ultrasonic anemometer. Only SRON provided low and high uncertainty bounds for wind speed estimates, not shown in this plot. Only includes wind speeds for nonzero quantified emissions, as some teams did not report wind speeds for non-detects.

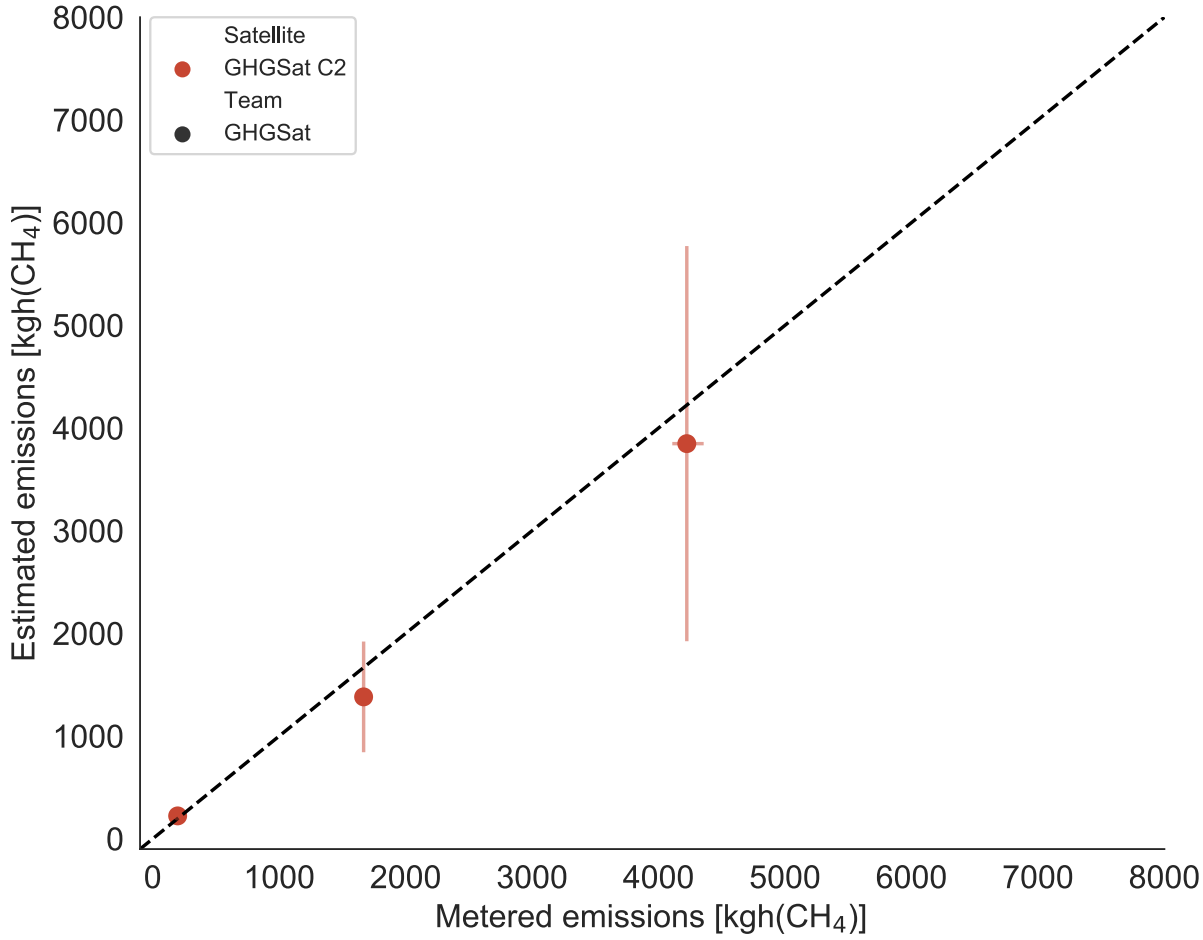

Figure 32. Stage 1 quantification performance for the GHGSat C2 satellite, with 1-sigma X and Y errorbars.

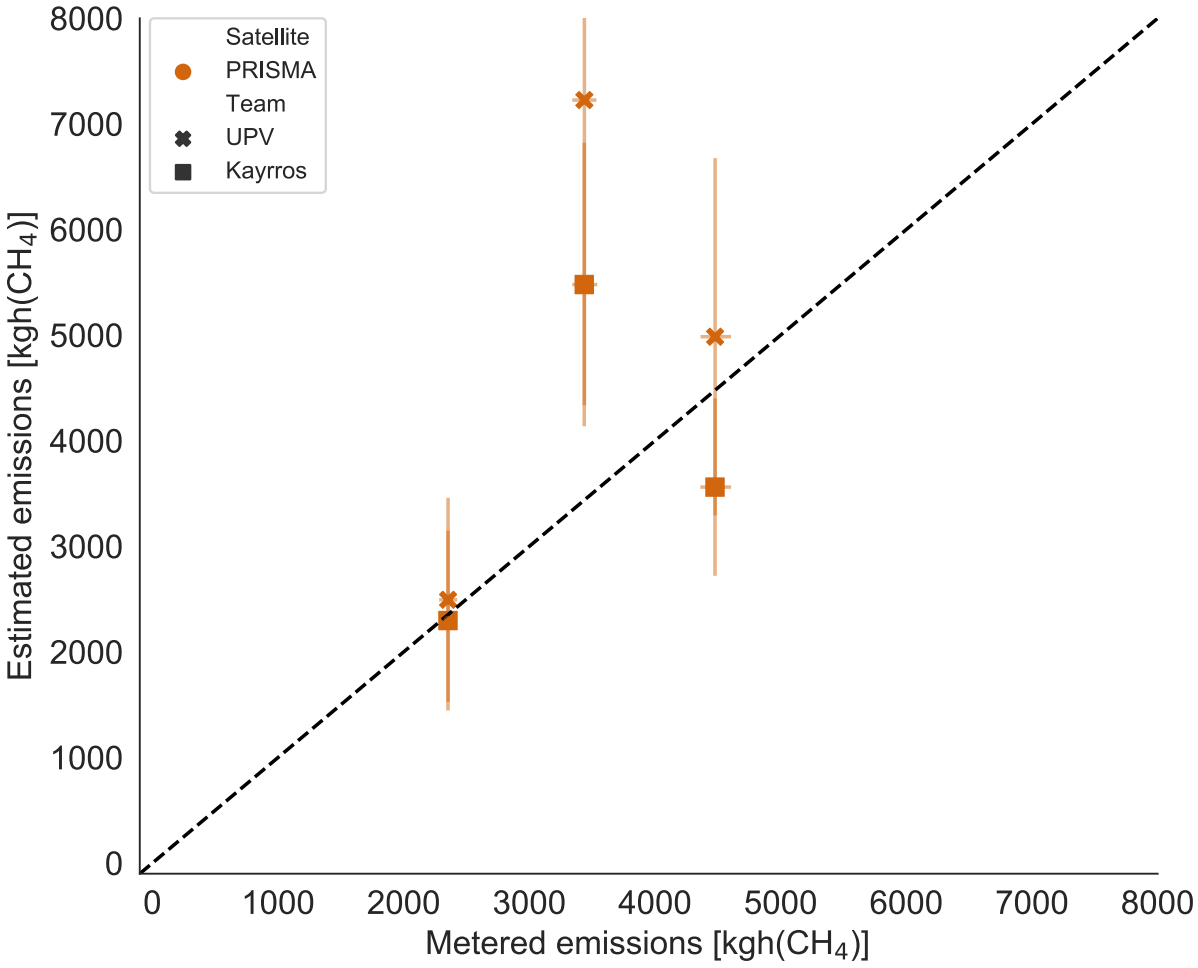

Figure 33. Stage 1 quantification performance for the PRISMA satellite, with 1-sigma X and Y errorbars.

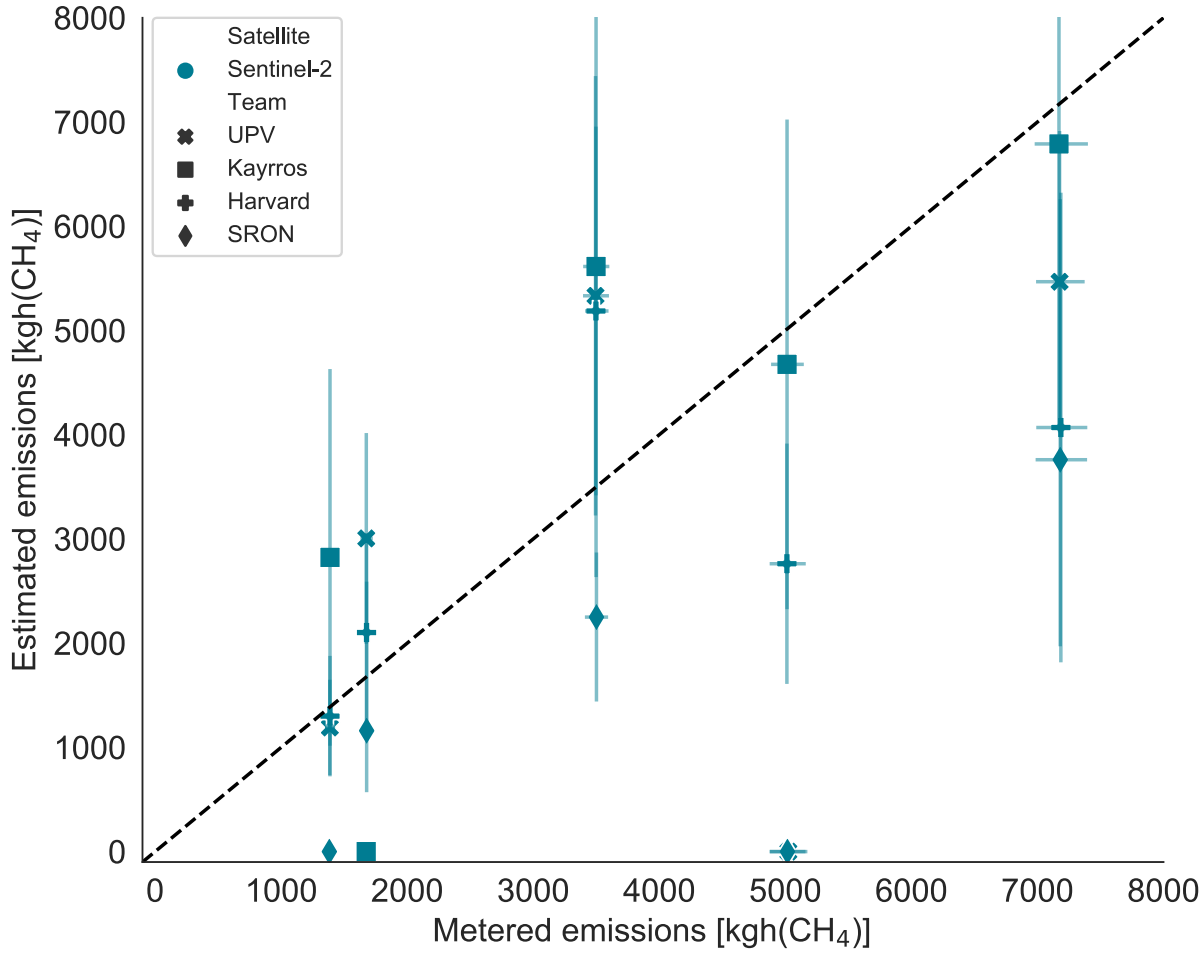

Figure 34. Stage 1 quantification performance for the Sentinel-2 satellite, with 1-sigma X and Y errorbars.

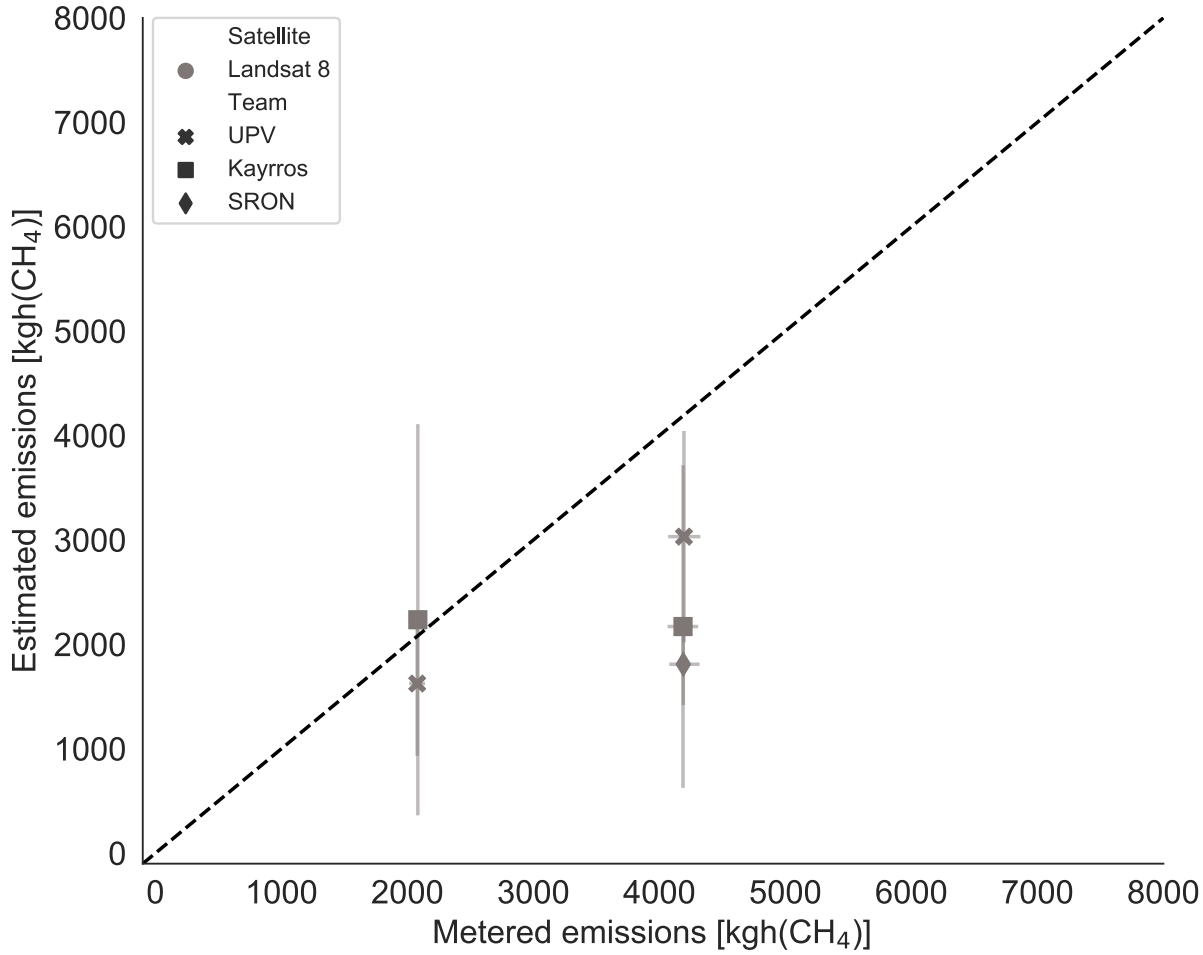

Figure 35. Stage 1 quantification performance for the Landsat 8 satellite, with 1-sigma X and Y errorbars.

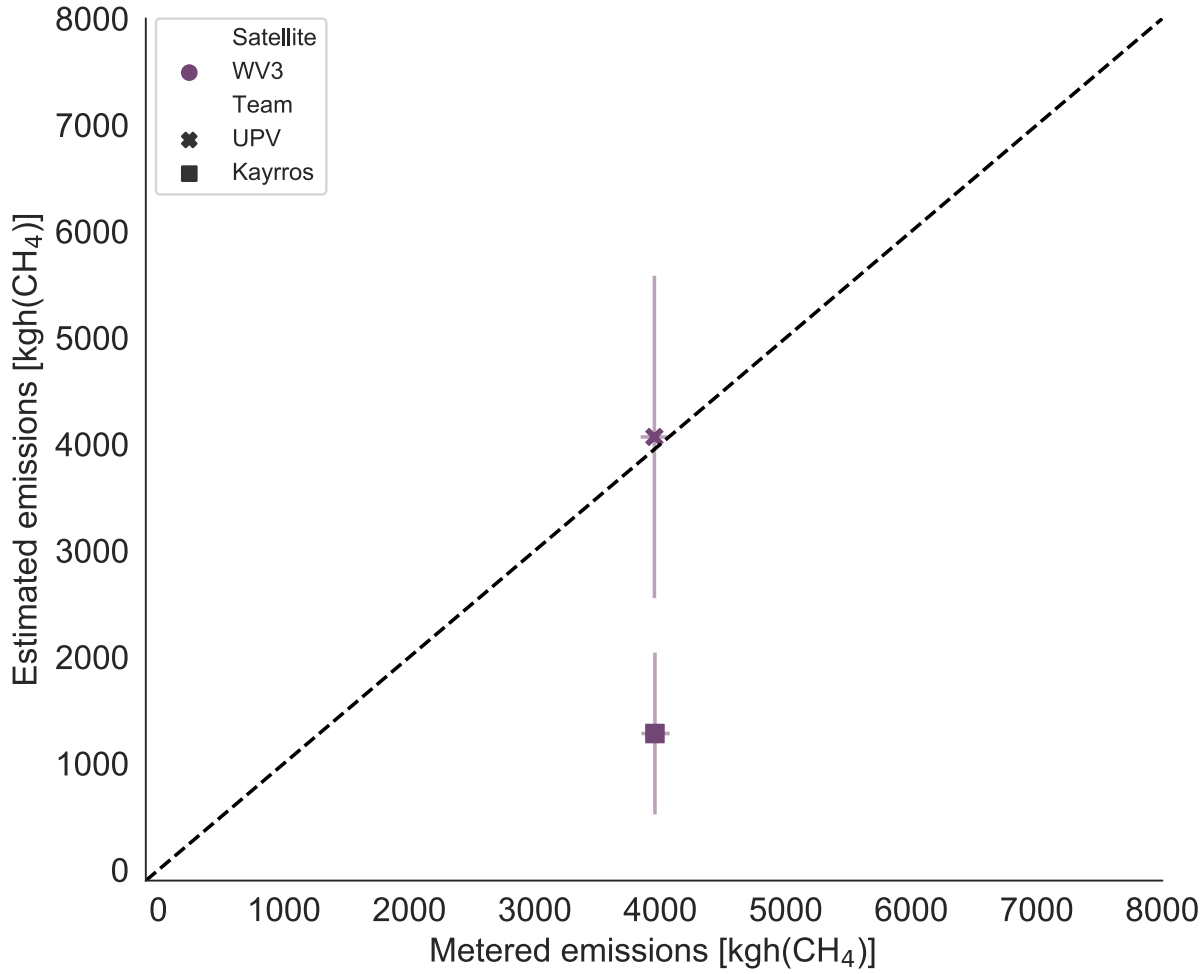

Figure 36. Stage 1 quantification performance for the WorldView 3 satellite, with 1-sigma X and Y errorbars.

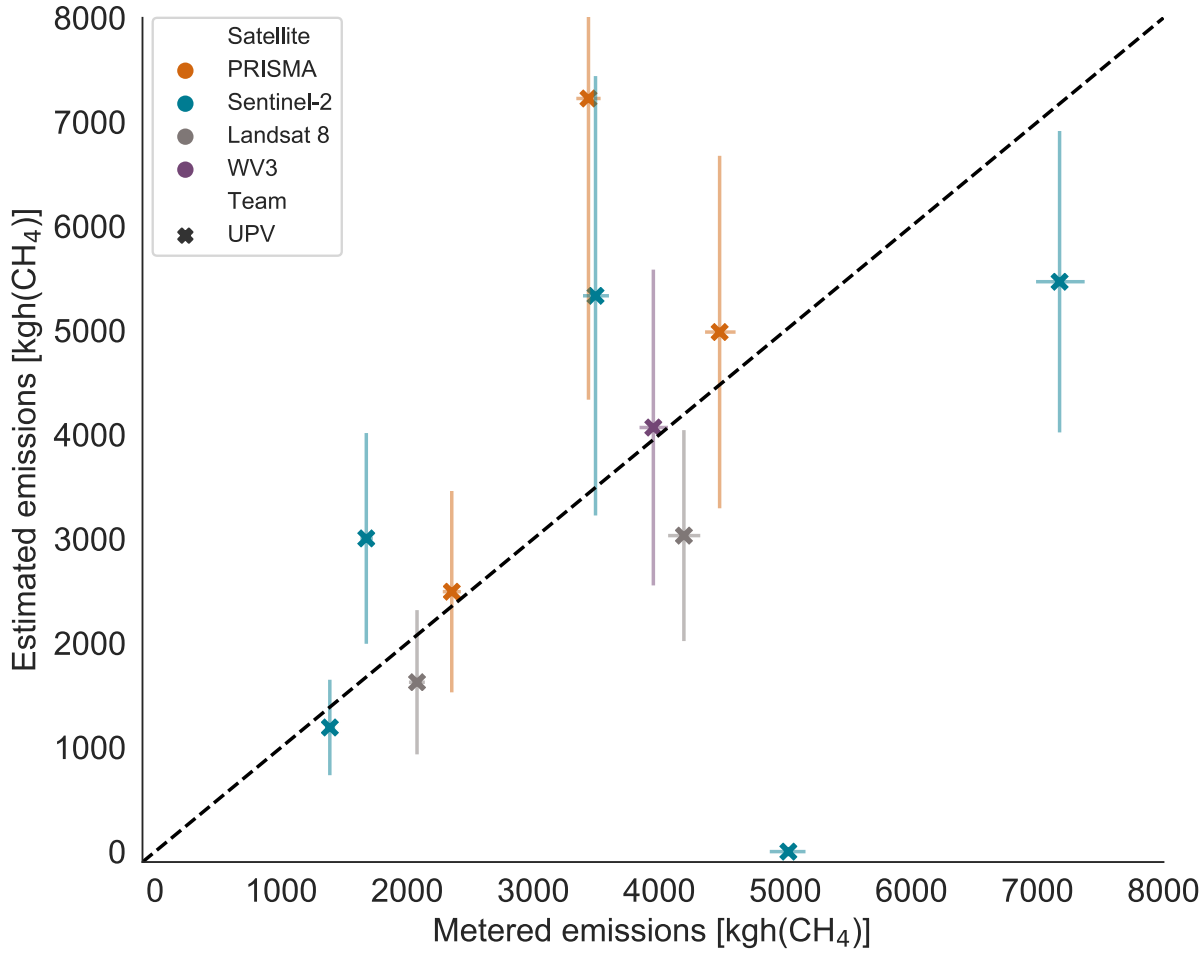

Figure 37. Stage 1 quantification performance for UP Valencia, with 1-sigma X and Y errorbars.

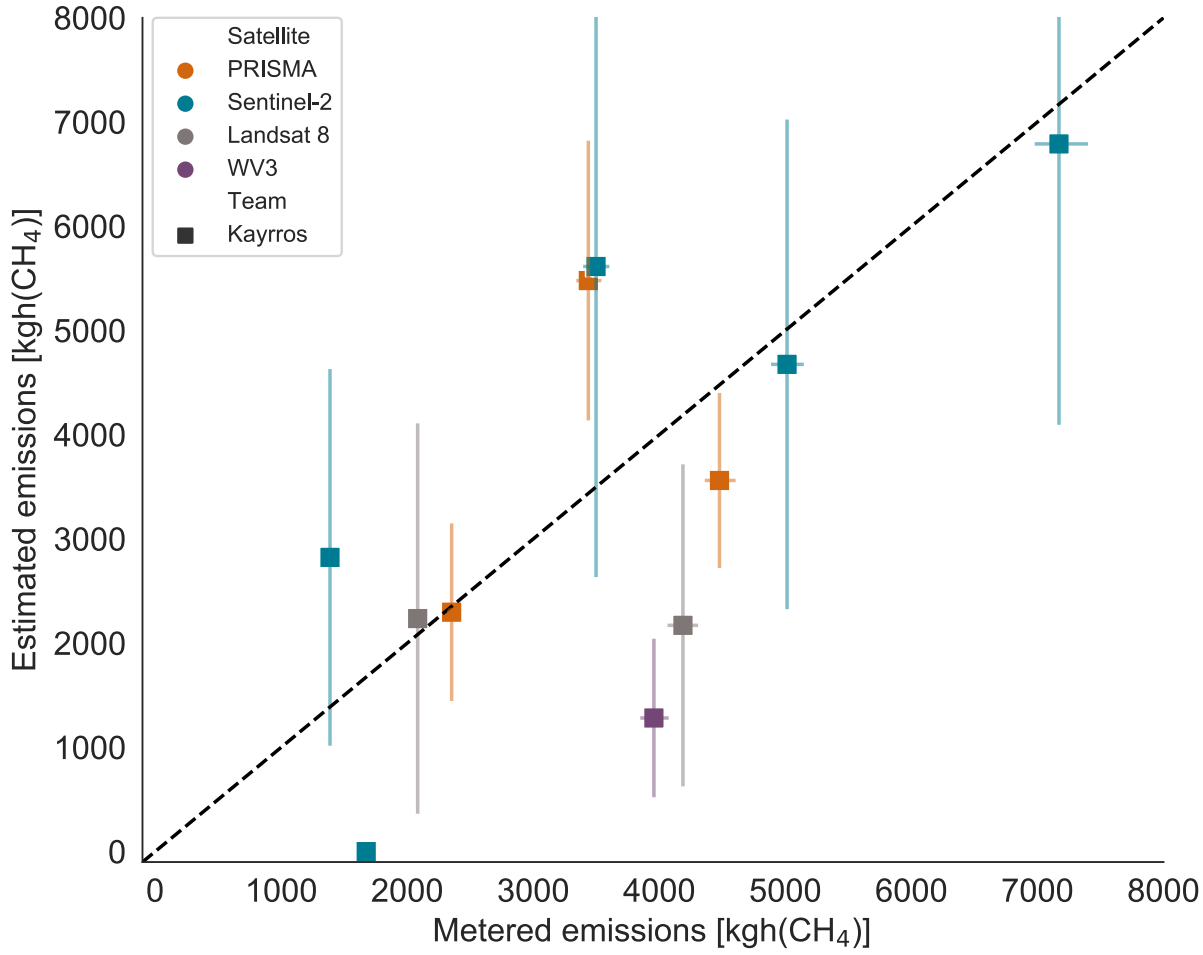

Figure 38. Stage 1 quantification performance for Kayrros, with 1-sigma X and Y errorbars.

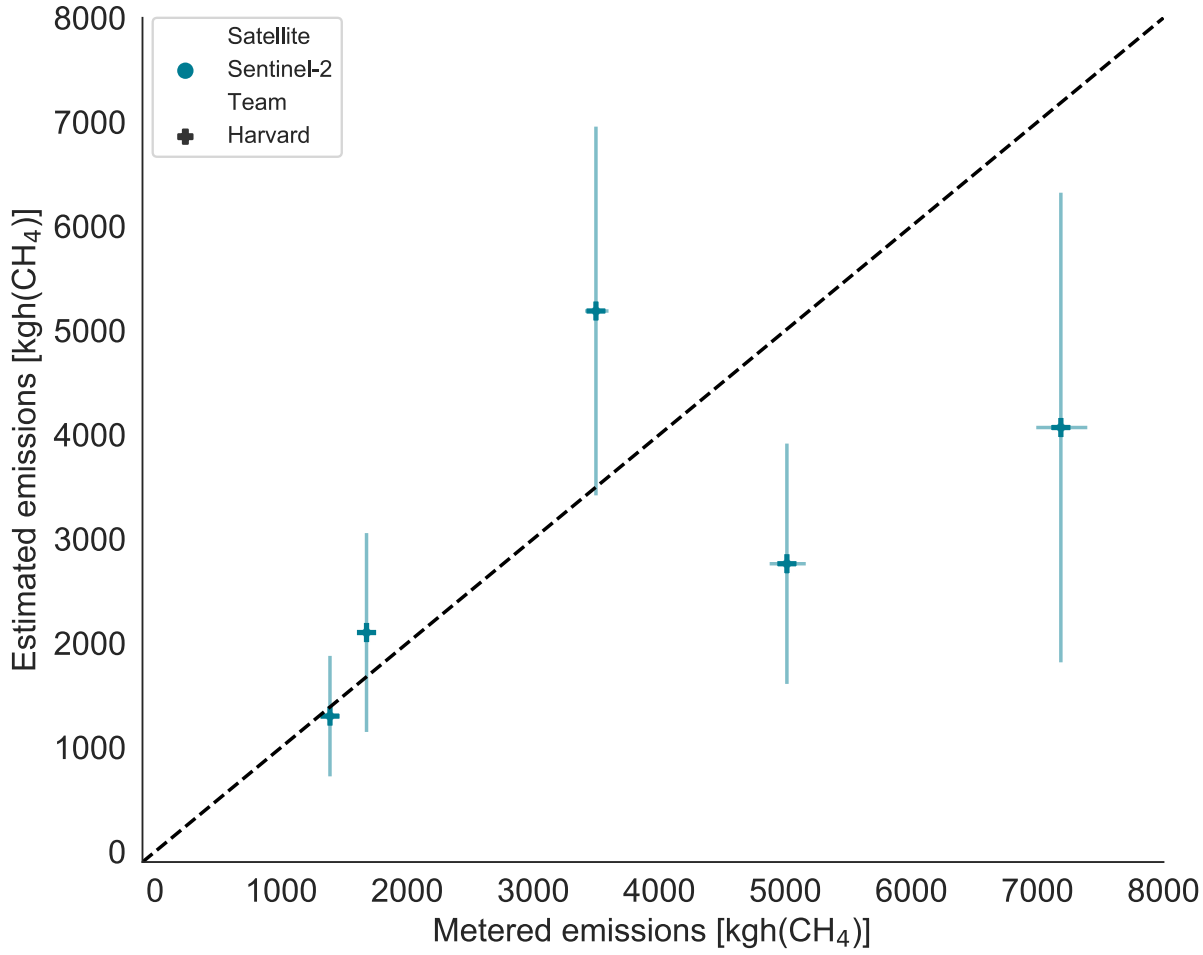

Figure 39. Stage 1 quantification performance for Harvard, with 1-sigma X and Y errorbars.

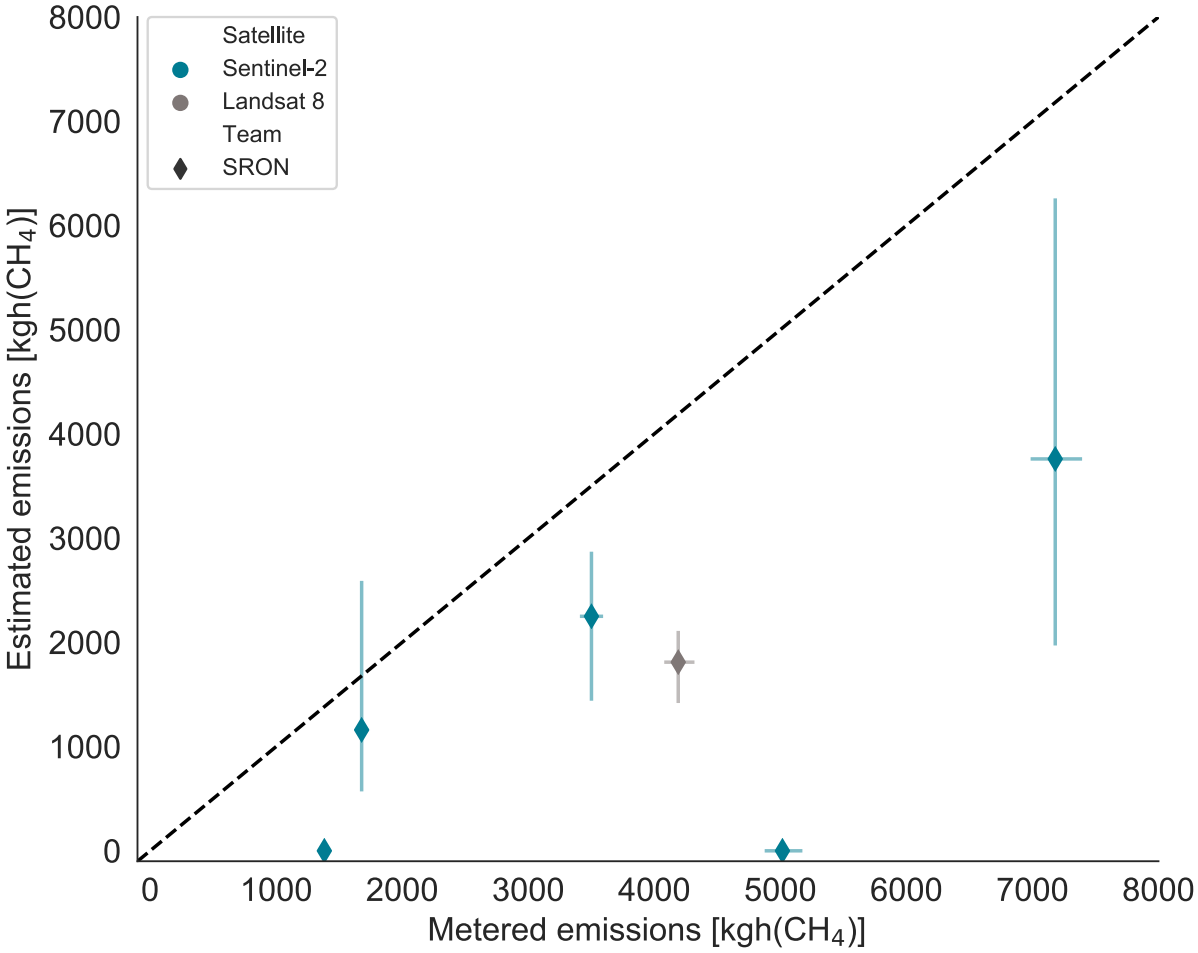

Figure 40. Stage 1 quantification performance for SRON, with 1-sigma X and Y errorbars.